Coherent evolution of *para*hydrogen induced polarisation using laser pump, NMR probe spectroscopy: theoretical framework and experimental observation

Meghan E. Halse[a,b*], Barbara Procacci[a,b], Sarah-Louise Henshaw[a,b], Robin N. Perutz[b*], and Simon B. Duckett[a,b*]

[a]*Centre for Hyperpolarisation in Magnetic Resonance, Department of Chemistry, York Science Park, University of York, Heslington, York, YO10 5NY, UK*

[b]*Department of Chemistry, University of York, Heslington, York, YO10 5DD, UK*

[*]Corresponding authors

Abstract

We recently reported a pump-probe method that uses a single laser pulse to introduce *para*hydrogen (p-H_2) into a metal dihydride complex and then follows the time-evolution of the p-H_2-derived nuclear spin states by NMR. We present here a theoretical framework to describe the oscillatory behaviour of the resultant hyperpolarised NMR signals using a product operator formalism. We consider the cases where the p-H_2-derived protons form part of an AX, AXY, AXYZ or AA'XX' spin system in the product molecule. We use this framework to predict the patterns for 2D pump-probe NMR spectra, where the indirect dimension represents the evolution during the pump-probe delay and the positions of the cross-peaks depend on the difference in chemical shift of the p-H_2-derived protons and the difference in their couplings to other nuclei. The evolution of the NMR signals of the p-H_2-derived protons, as well as the transfer of hyperpolarisation to other NMR-active nuclei in the product, is described. The theoretical framework is tested experimentally for a set of ruthenium dihydride complexes representing the different spin systems. Theoretical predictions and experimental results agree to within experimental error for all features of the hyperpolarised ^1H and ^{31}P pump-probe NMR spectra. Thus we establish the laser pump, NMR probe approach as a robust way to directly observe and quantitatively analyse the coherent evolution of p-H_2-derived spin order over micro-to-millisecond timescales.

Graphical Abstract
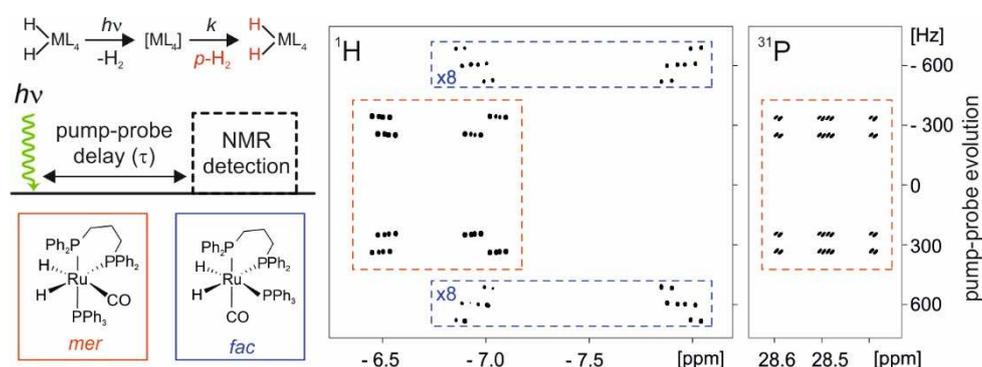
Highlights

- Experimental observation of the coherent evolution of *para*hydrogen-derived spin states over a micro-to-millisecond timescale using a laser-pump, NMR probe approach.

- Development of a first-principles theoretical model to describe the coherent evolution of p-H_2-derived spin states under both chemical and magnetic inequivalence of the p-H_2-derived protons.

- Experimental validation of the theoretical model with reference to a range of ruthenium dihydride complexes that provide access to different spin topologies.

- Theoretical prediction and experimental observation of transfer of hyperpolarisation from a pair of p-H_2-derived protons to a third nucleus (^{31}P) in the high-field regime.

I.   Introduction

Hyperpolarisation is an increasingly important area of development in magnetic resonance, particularly in fields such as biomedical NMR and MRI, where applications are often sensitivity limited.[1] Hyperpolarisation methods boost the sensitivity of magnetic resonance by increasing the population imbalance between nuclear energy levels from a few ppm/T at thermal equilibrium up to as much as several tens of percent. Dozens of hyperpolarisation schemes have been proposed. The most widely used of these are based on dynamic nuclear polarisation (DNP),[2-5] spin-exchange optical pumping (SEOP),[6] and parahydrogen-induced polarisation (PHIP).[7-10] These hyperpolarisation techniques differ in both the source of their polarisation and the method of transfer to the target nuclei.

In this work we focus on PHIP, which is a general term that refers to all methods where the source of polarisation is *para*hydrogen (p-H_2). *Para*hydrogen is the nuclear spin isomer of molecular hydrogen in which the pair of spin-1/2 ^1H nuclei form a singlet state. The use of p-H_2 as a route to hyperpolarisation was first predicted by Bowers and Weitekamp in 1986 [8] and exemplified shortly after.[7, 9] This method takes advantage of the relatively easy route to prepare H_2 in this thermodynamically preferred form. However, p-H_2 has no net angular momentum and so is NMR silent. If the symmetry of the chemical and/or magnetic environments of the ^1H nuclei in p-H_2 is broken, for example by means of transporting them through oxidative addition at a metal centre into inequivalent environments, the singlet state will evolve into NMR observable triplet states in the product molecule. The NMR signals of the former p-H_2-nuclei in the product can be enhanced by several orders of magnitude.[7, 11, 12] In some cases, NMR signal enhancements can also be observed for other NMR-active nuclei in the product molecule due to spontaneous or radio-frequency (*rf*) driven polarisation transfer from the protons originally on p-H_2.[10, 13-18] This polarisation transfer phenomenon is harnessed in the signal amplification by reversible exchange (SABRE) approach, which uses a reversible exchange reaction to catalytically transfer polarisation from p-H_2-derived protons to nuclei in a target substrate molecule without chemical alteration of the substrate.[10, 19] *Para*hydrogen is a particularly attractive source of hyperpolarisation because it is relatively cheap and easy to produce by cooling H_2 gas in the presence of a paramagnetic species (e.g. activated charcoal or iron oxide). Once generated at low temperature

(typically between 20 – 77 K depending on the desired level of p-H_2 enrichment) p-H_2 can be stored at room temperature for weeks or even months.[12]

Since the initial experimental demonstrations by Bowers and Weitekamp,[7] and Eisenberg and co-workers,[9] PHIP has become a valuable tool for the study of reactivity in inorganic and organic chemistry, particularly for elucidating reaction mechanisms and for the identification of intermediates in hydrogenation chemistry.[20-23] More recently, PHIP and SABRE have been used for the development of hyperpolarised contrast agents for clinical MRI.[24-26]

In most PHIP experiments, thermally-activated reactions are used to build-up the population of hyperpolarised molecules over a period of seconds. The asynchronous nature of this approach means that the p-H_2 hyperpolarisation that is detected corresponds to a time-averaged response. Thus information about the coherent evolution of the p-H_2 singlet state into NMR-observable triplet states is lost.[11] It should be noted that the coherent evolution of the p-H_2-derived magnetic states in a product molecule could theoretically be observed following a thermally activated reaction if a suitable radio frequency (rf) irradiation scheme is applied during the reaction period to suppress evolution under chemical shift and/or spin-spin coupling. This approach was used by Goldman and Johannesson to maximise the efficiency of transfer of p-H_2-derived ^1H spin order to a neighbouring heteronucleus (e.g. ^{13}C) in the product molecule.[27]

Another approach is to use a photochemical reaction to unlock the hyperpolarisation potential of p-H_2. In this method, a reaction with p-H_2 is initiated photochemically within the NMR spectrometer.[28] Duckett, Perutz and co-workers have shown that *in situ* photolysis can be used to help elucidate chemical mechanisms and to observe intermediates in photochemically-activated reactions involving p-H_2.[28-31] In addition, this approach has also been used to assess the purity of the p-H_2-derived singlet state upon oxidative addition of p-H_2 to a transition-metal complex.[32, 33] Building on this previous work, we recently demonstrated a new method that harnesses p-H_2 hyperpolarisation in a synchronised way.[34] This approach was inspired by pump-probe methods that combine photochemical excitation with optical detection techniques such as UV/vis,[35, 36] IR,[37] and Raman spectroscopy,[38-40] to perform time-resolved spectroscopy of reactivity on timescales from milliseconds down to femtoseconds. In the analogous time-resolved NMR experiment, the sample is pumped

5

photochemically using a single *in situ* laser pulse that is synchronised with the NMR spectrometer. After a well-defined pump-probe delay a radio-frequency (*rf)* probe pulse is applied and the NMR response is recorded. The excess (unreacted) p-H$_2$ in solution is NMR-silent; therefore, in the absence of any thermal reactivity of the p-H$_2$, the hyperpolarised NMR response excited by the probe pulse corresponds exclusively to the products of the reaction with p-H$_2$ that was initiated photochemically by the laser pump pulse. The time delay between the laser pump and the NMR probe is readily and precisely controlled by the 200 ns clock on the spectrometer, allowing for short pump-probe delays on the order of the duration of the NMR pulse (i.e. 10 μs).[34] Typically, a single scan pump-probe NMR spectrum provides sufficient signal-to-noise for analysis; however, signal averaging is possible in cases where the hyperpolarised species of interest is present at an extremely low concentration. The time-resolved NMR experiment with p-H$_2$ hyperpolarisation presents the opportunity to (a) study chemical reactivity on micro-to-millisecond timescales,[41] and (b) observe the coherent evolution of the p-H$_2$-derived spin states directly by conversion via *rf* excitation into observable NMR magnetisation. Thus this photochemical pump, NMR probe method provides a unique test-bed for exploring the evolution of the p-H$_2$-derived spin states in the product molecule. Of particular interest is the potential to directly probe the transfer of polarisation from the former-p-H$_2$ ^{1}H's to other nuclei, either through spontaneous transfer in the strong coupling regime or via *rf*-driven transfer.

*Para*hydrogen is of interest in NMR spectroscopy not only because of the potential for hyperpolarisation but also as an example of a nuclear singlet state. Singlet states are important in NMR because they can be exploited to prepare molecules with so-called long-lived states (LLS) [42] and long-lived coherences (LLC).[43] LLS and LLC have a wide range of potential applications, such as the preservation of NMR hyperpolarisation and line-narrowing in solution-state NMR. The theory behind the preparation and evolution of LLS and LLC has been discussed extensively [42, 44-54] and shares many features with the evolution of p-H$_2$ hyperpolarisation. The fact that p-H$_2$ is only one of a large number of molecules that can contain nuclei in long-lived nuclear spin states suggests that the applications of the photochemical pump, NMR probe methodology are not limited to reactions involving H$_2$. The reactivity of any molecule prepared in a long-lived state could be monitored using this time-resolved NMR approach as long as the reaction can (a) be initiated photochemically, and (b) the symmetry of the nuclei that

make up the long-lived state is broken in an appropriate way in the reaction product. This feature of the method is particularly interesting since it has been shown that various hyperpolarisation methods, including dissolution DNP [55, 56] and SABRE [57-59] can be used to prepare nuclei in a range of molecules in a hyperpolarised long-lived state.

In this paper we use the photochemical pump, NMR probe method to directly observe and analyse the effects of the coherent magnetic evolution of the p-H$_2$-derived spin states on the observed hyperpolarised NMR signals. Starting from the standard description of p-H$_2$, we develop analytical expressions for the coherent evolution of the p-H$_2$-derived states following spin-conserved insertion of the protons from p-H$_2$ into a range of commonly-occurring spin topologies. The examples studied here include: an AX spin system where the former-p-H$_2$ ^{1}H nuclei are chemically inequivalent in the product, AXY and AXYZ spin systems where the chemically inequivalent hydrides in the product (AX) couple differently to one or more other nuclei (Y and Z), and an AA'XX' spin system, where the p-H$_2$-derived hydrides in the product (AA') are chemically equivalent but are magnetically inequivalent due to the difference in scalar couplings to a second pair of nuclei (XX'). The successful detection of p-H$_2$ hyperpolarisation on both the p-H$_2$–derived hydrides and on other nuclei (e.g. ^{31}P) is described. These theoretical predictions are verified experimentally through the direct observation of the evolution of the p-H$_2$-enhanced ^{1}H and ^{31}P NMR signals in a range of ruthenium dihydride complexes. The effect of NMR relaxation on the observed NMR signals is discussed and the relaxation rates for our example systems are reported.

II.   Theory

A.   Laser pump, NMR probe spectroscopy with *para*hydrogen hyperpolarisation

The laser pump, NMR probe experiment, as applied to the oxidative addition of p-H$_2$ to a transition metal complex, is illustrated schematically in Figure 1a.[34]   A single laser pulse is applied, *in situ*, to an optically dilute solution of a transition metal dihydride complex in the presence of a large excess of p-H$_2$. The laser pulse initiates prompt reductive elimination of dihydrogen from the metal dihydride complex to form an unsaturated intermediate, which reacts with the p-H$_2$ in solution to reform the original dihydride complex, now with magnetically-labelled hydrides (Scheme 1). The schemes in this paper assume an octahedral product geometry with, therefore, a clear *cis/trans* ligand distinction. However, the principles of this approach are in fact more general and

7

we have reported *in situ* photochemistry with *p*-H$_2$ for other geometries.[28, 60]
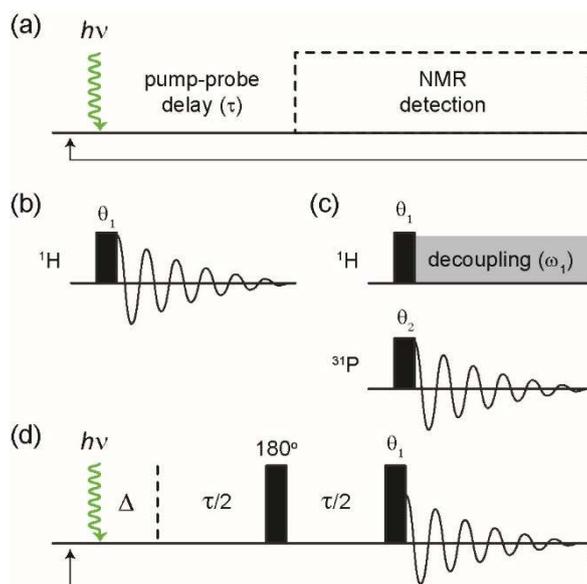
Figure 1. (a) Typical laser pump, NMR probe experiment: a single laser shot is followed, after a well-defined pump-probe delay (τ), by NMR detection. The NMR detection block contains: (b) a one-pulse ^{1}H NMR detection scheme, or (c) an X-channel NMR detection scheme with an optional *rf* pulse, θ_1, and/or heteronuclear decoupling is applied to the ^{1}H channel; (d) an echo-based measurement to determine zero-quantum relaxation times, where $\Delta = 1/(4\delta\nu)$ in the chemical inequivalent case, or $\Delta = 1/(4\Delta J)$ in the magnetic inequivalent case.
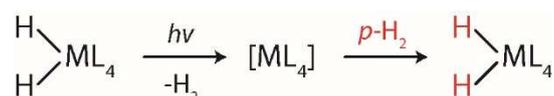
Scheme 1. A single laser shot is used to eliminate dihydrogen and form a highly reactive intermediate, which then oxidatively adds *p*-H$_2$ to reform the starting material with magnetically labelled hydrides (red).

After a well-defined pump-probe delay, τ, a suitable NMR detection pulse sequence is applied (Figure 1) and a single high-resolution NMR spectrum is recorded. The evolution of the system following the laser pulse is probed by acquiring a series of pump-probe NMR spectra for different delays, τ, where each 1D NMR spectrum is associated with a single laser pulse. This series of 1D NMR spectra can be Fourier Transformed to produce a 2D pump-probe NMR spectrum, where the indirect dimension provides information about the evolution of the system during the pump-probe delay, τ.

In contrast to other time-resolved spectroscopies, pump-probe NMR spectra can contain information about both the chemical evolution of the system (e.g. the kinetics of the oxidative addition of p-H$_2$ to the metal complex) and the coherent evolution of the initial p-H$_2$-derived state into observable magnetisation. The details of the coherent magnetic evolution will depend on the spin topology of the metal dihydride complex. In this work we consider complexes where the p-H$_2$ addition rates are orders of magnitude faster than any magnetic evolution. Hence, we can assume that any changes in the NMR response as a function of the pump probe delay are due exclusively to magnetic evolution under coupling interactions, chemical shift or relaxation.

B.   Magnetic evolution during pump-probe delay

The theory of *para*hydrogen hyperpolarisation[8] was reviewed by Natterer and Bargon in 1997 [11], by Bowers in 2007 [61], and by Green *et al*. in 2012.[12] Here we describe the basic principles of p-H$_2$ hyperpolarisation to make the manuscript self-contained and to establish a consistent nomenclature. We note that the theoretical framework used here is consistent with that originally developed by Bowers and Weitekamp [7, 8, 62] and subsequently expanded to explore the use of field cycling and *rf* irradiation for the efficient transfer of p-H$_2$-derived hyperpolarisation to other nuclei.[11]

In a standard PHIP experiment, the reaction with p-H$_2$ is initiated thermally and the p-H$_2$-labelled product is generated over a period of seconds. In this case, the observed NMR response is averaged over the reaction period between NMR excitation steps. In our approach, the photochemical pump step generates an ensemble of p-H$_2$-labelled product molecules on a microsecond timescale. This allows us to validate the theoretical framework through direct observation of the coherent evolution of the p-H$_2$-derived spin states in the resulting product over a micro-to-millisecond time window. In particular, we validate the predicted evolution of the zero-quantum coherences, something that has not been achieved using the standard time-averaged PHIP approach. We note that this laser pump, NMR probe methodology is analogous to the laser-initiated chemically induced dynamic nuclear polarisation experiment (photo-CIDNP), in which a spin-correlated radical pair is used to generate NMR signal enhancements on the order of 10^2. Coherent magnetic oscillations have been observed with CIDNP [63-66] and modelled using numerical simulations of the coherent evolution of the system driven by differences in chemical shift and/or *J* coupling interactions.[66] Photo-CIDNP has been used to

observe short-lived radicals and to monitor reactivity on millisecond to second timescales.[67-70]

As stated earlier, p-H$_2$ is the spin isomer of H$_2$ that exists in a nuclear singlet state. In the product operator basis, this state can be described by the density matrix, $\rho_{p\text{H}_2}$:

$$\rho_{p\text{H}_2} = \tfrac{1}{4}E - \mathbf{I} \cdot \mathbf{S} = \tfrac{1}{4}E - \tfrac{1}{2}\left(2I_zS_z + 2I_yS_y + 2I_xS_x\right) \tag{1}$$

where $\mathbf{I} = \{I_x, I_y, I_z\}$ and $\mathbf{S} = \{S_x, S_y, S_z\}$ are the total spin angular momentum operators (with associated Cartesian components) for the two ^{1}H nuclei in p-H$_2$ and E is the identity operator. Without any loss of generality, we neglect the identity operator, which does not give rise to observable NMR signal, and consider only the second term in Eq. 1. For convenience, we use standard notation [11] to divide this term into two parts: the longitudinal term: $\tfrac{1}{2}(2I_zS_z)$ and the transverse term, zero-quantum-x (ZQ_x, Eq. 2).

$$ZQ_x = \tfrac{1}{2}\left(2I_yS_y + 2I_xS_x\right) \tag{2}$$

If the ^{1}H nuclei are magnetically equivalent, as is the case in molecular hydrogen, this state is invariant to rotation by an rf pulse and is NMR silent. It is only by breaking the symmetry of the ^{1}H environments that we can exploit p-H$_2$ to obtain orders-of-magnitude increases in NMR signal amplitudes. In p-H$_2$-enhanced NMR, the required break in symmetry is typically achieved through the pairwise addition of p-H$_2$ to a metal complex or through spin-conserved hydrogenation of an unsaturated substrate.[11, 12] In the examples in this paper we use the former method but our results are not limited to this case, nor are they limited to the use of p-H$_2$ as the source of the hyperpolarised singlet state. For example, a hyperpolarised ^{15}N-^{15}N singlet state could be used.[59]

It has been shown previously that the p-H$_2$ singlet state can be conserved upon oxidative addition of p-H$_2$ at a metal centre.[33] If we assume this is the case and that the former p-H$_2$ nuclei are placed into magnetically different environments in the product, the p-H$_2$-derived singlet state will evolve into observable triplet states under the influence of the internal spin Hamiltonian, H, according to the Liouville-von-Neumann equation (Eq. 3), where the density matrix at $t = 0$ is equal to the $para$hydrogen singlet state, $\rho(0) = \rho_{p\text{H}_2}$. Note here we are using the common convention in NMR where H is written in units of angular frequency.

$$d\rho(t)/dt = -i[H, \rho(t)] \tag{3}$$

The evolution of the system beyond this point will depend on the form of the internal spin Hamiltonian, H.

1. *Chemical inequivalence (AX, AXY, AXYZ)*

In our first example we consider a situation where the p-H$_2$-derived protons are 'instantaneously' (i.e. on a timescale much faster than any magnetic evolution of the system) placed into two chemically distinct environments (Scheme 2a and 2b). The weakly-coupled AX case has been solved previously [8] and is provided in the supporting information.
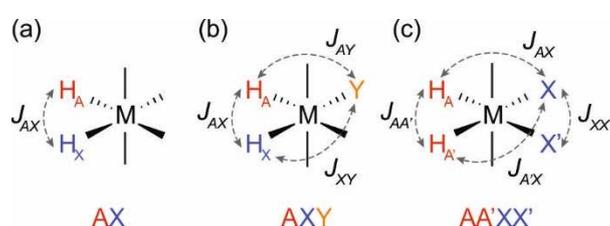
Scheme 2. Coupling constants in (a) AX, (b) AXY and (c) AA'XX' spin systems.

Here we briefly summarise the result for an AXY spin system, where the p-H$_2$-derived protons are placed into chemically inequivalent environments ($\delta\omega = \omega_A - \omega_X \neq 0$) in the product and experience additional but different couplings to a third nucleus, Y ($\Delta J = J_{AY} - J_{XY} \neq 0$). This situation is encountered when a single NMR-active heteronucleus (e.g. ^{31}P) is coordinated to the metal centre *trans* to one of the hydride ligands (Scheme 2b) and reflects a common situation in inorganic chemistry. In this case, the relevant coupling is the difference between the couplings of each of the hydrides and the third nucleus: $\Delta J = J_{AY} - J_{XY}$.

The AXY class of spin system is of particular interest when considering the transfer of p-H$_2$-derived ^{1}H spin order to other nuclei in the product molecule. This transfer of polarisation can occur spontaneously or under the influence of *rf* irradiation depending on the spin topology of the product molecule and the experimental conditions employed. Many different approaches have been developed to optimise the transfer of spin order, including field cycling,[71] *rf* irradiation,[13, 15-17, 72] exchange reactions,[10] and combinations thereof. In the following we focus specifically on the high-field case where the p-H$_2$-derived protons are weakly coupled in the product and the difference in coupling to the third nucleus is significant (tens of Hz) but nevertheless is weaker than

the difference in chemical shift between the p-H$_2$-derived protons (hundreds of Hz). The full internal spin Hamiltonian for the spin system in this case is presented in Eq. 4, where ω_A, ω_X, and ω_Y are the Larmor frequencies and I_z, S_z, and T_z are the longitudinal spin angular momentum operators for the A, X, and Y spins, respectively. J_{AX}, J_{AY} and J_{XY} are the coupling constants between the nuclei.

$$H_{AXY} = -\omega_A I_z - \omega_X S_z - \omega_Y T_z + 2\pi J_{AX} I_z S_z + 2\pi J_{AY} I_z T_z + 2\pi J_{XY} S_z T_z \qquad (4)$$

The time-dependent density matrix under the influence of this Hamiltonian, where the initial density matrix is given by Eq. 1, can be obtained using Eq. 3 to obtain the expression in Eq. 5. Here we have used the Bloch approach to include the effects of NMR relaxation through the introduction of effective relaxation rates, $R_{1,I_z S_z}$, and $R_{2,ZQ}$, which describe the average NMR relaxation behaviour of the longitudinal two-spin-order term and the zero-quantum coherences, respectively. Note here we use the shorthand for the zero-quantum-y coherence, which is defined as $ZQ_y = \frac{1}{2}(2I_y S_x - 2I_x S_y)$.

$$\rho_{AXY}(\tau) = -a_1(\tau)\tfrac{1}{2}(2I_z S_z) - a_2(\tau)2ZQ_x\left(\tfrac{1}{2} + T_z\right) - a_3(\tau)2ZQ_x\left(\tfrac{1}{2} - T_z\right)$$

$$+a_4(\tau)2ZQ_y\left(\tfrac{1}{2} + T_z\right) + a_5(\tau)2ZQ_y\left(\tfrac{1}{2} - T_z\right) \qquad (5a)$$

where

$$a_1(\tau) = \exp\left(-R_{1,I_z S_z}\tau\right) \qquad (5b)$$

$$a_2(\tau) = \tfrac{1}{2}\cos\left((\delta\omega + \pi\Delta J)\tau\right)\exp\left(-R_{2,ZQ}\tau\right) \qquad (5c)$$

$$a_3(\tau) = \tfrac{1}{2}\cos\left((\delta\omega - \pi\Delta J)\tau\right)\exp\left(-R_{2,ZQ}\tau\right) \qquad (5d)$$

$$a_4(\tau) = \tfrac{1}{2}\sin\left((\delta\omega + \pi\Delta J)\tau\right)\exp\left(-R_{2,ZQ}\tau\right) \qquad (5e)$$

$$a_5(\tau) = \tfrac{1}{2}\sin\left((\delta\omega - \pi\Delta J)\tau\right)\exp\left(-R_{2,ZQ}\tau\right) \qquad (5f)$$

The longitudinal two-spin-order term, $\frac{1}{2}(2I_z S_z)$, commutes with the Hamiltonian (Eq. 4) at all points in time and so only evolves due to relaxation (Eq. 5b). The amplitudes of the ZQ coherences oscillate during the pump probe delay at angular frequencies of $\delta\omega \pm \pi\Delta J$. In the absence of a difference in coupling to a third nucleus (i.e. for an isolated AX spin

system), this oscillation frequency is simply the difference in chemical shift between the *p*-H$_2$-derived protons. The presence of couplings to additional nuclei will modulate this oscillation frequency in a manner that is directly analogous to that of the classic doublet observed in a 1D NMR spectrum, except here the doublet is centred at a frequency equal to the difference in chemical shift between the hydrides, $\delta\omega/2\pi$, and the splitting is the difference in *J* coupling between each of the hydrides and the third nucleus, ΔJ. If more than one additional nucleus couples differently to the hydrides, we would expect to observe additional frequency components in the oscillation due to the additional *J* coupling differences. The values and relative amplitudes of these frequency components will follow the well-known rules of multiplicity from standard 1D NMR, and the splittings will correspond to the difference in *J* coupling to the two hydrides.

2. *Magnetic inequivalence (AA'XX')*

In our second example, we consider the case where the *p*-H$_2$-derived protons are placed into two chemically equivalent environments that are made magnetically inequivalent by virtue of different scalar couplings to a second pair of nuclei (AA'XX' system). This situation is typically encountered when there are two chemically equivalent heteronuclei coordinated to the metal centre in the same plane as the hydrides (Scheme 2c). The difference in scalar coupling comes from the difference in the *cis* and *trans* couplings between each of the hydrides and the heteronuclei ($\Delta J = J_{trans} - J_{cis} = J_{A'X} - J_{AX} = J_{AX'} - J_{A'X'}$) and can be quite large (tens of Hz for ^{1}H -^{31}P couplings).

The features of an AA'XX' spin system in a standard NMR spectrum were analysed by Pople *et al.* in 1957.[73] More recently, Theis *et al.* have extended the Pople description to include the effects of *p*-H$_2$ hyperpolarisation for the case where the difference in coupling between the *p*-H$_2$-derived A nuclei and the X nuclei is smaller than the homonuclear AA' and XX' couplings ($J_{AA'} + J_{XX'} \gg \Delta J$).[74, 75] In this case, the transfer of spin-order from the *p*-H$_2$ derived protons (AA') to the heteronuclei (XX') is driven by either the application of a low-power *rf* spin-lock field in resonance with the homonuclear couplings ($J_{AA'} + J_{XX'}$) in the high-field case [74] or by level anti-crossings in the ultra-low-field case.[75-77] Similarly, high-field polarisation transfer from *p*-H$_2$-derived A spins to X spins in an AA'XX' system has been demonstrated experimentally using high-power *rf* irradiation and analysed in the doubly rotating frame in terms of *rf*-induced level anti-crossings by Pravdivtsev *et al.*[78] In the situation considered in this paper $J_{AA'} +$

$J_{XX'} < \Delta J_{AA'XX'}$ and we explore the coherent magnetic evolution that proceeds in the high-field case in the absence of *rf* irradiation.

The time-independent Hamiltonian for an AA'XX' spin system is given in Eq. 6, where ω_A and ω_X are the Larmor frequencies of the *p*-H$_2$-derived protons (A and A') and the X nuclei, respectively, $J_{AA'}$ is the coupling between the A nuclei, $J_{XX'}$ is the coupling between the X nuclei, $J_{cis} = J_{AX} = J_{A'X'}$ and $J_{trans} = J_{AX'} = J_{A'X}$ are the couplings between A and X nuclei and $(\Delta J = J_{trans} - J_{cis} = J_{A'X} - J_{AX} = J_{AX'} - J_{A'X'}$. **I**, **S**, **T**, and **R** are the total angular momentum operators (with associated Cartesian coordinates) for the A, A', X and X' spins, respectively.

$$H_{AA'XX'} = -\omega_A(I_z + S_z) - \omega_X(T_z + R_z) + 2\pi J_{AA'}\mathbf{I} \cdot \mathbf{S} + 2\pi J_{XX'}\mathbf{T} \cdot \mathbf{R}$$

$$+2\pi J_{trans}(I_z T_z + S_z R_z) + 2\pi J_{cis}(I_z R_z + S_z T_z) \qquad (6)$$

If we assume that the homonuclear X-X coupling is very small, $J_{XX'} \ll J_{AA'}$ and $J_{XX'} \ll \Delta J$, the density matrix as a function of time can be written as in Eq. 7.

$$\rho^{AA'XX'}(\tau) = -b_1(\tau)\tfrac{1}{2}(2I_{1z}I_{2z})$$

$$-b_2(\tau)ZQ_x - b_3(\tau)2ZQ_y(T_z - R_z) - b_4(\tau)2\tfrac{1}{2}(I_z - S_z)(T_z - R_z) \qquad (7)$$

If the homonuclear coupling between the *X* spins is <u>not</u> negligible, additional magnetic states will be created through evolution under the influence of the fourth term of Eq. 6. However, when the evolution of the system due to the strong coupling between the *X* nuclei can be neglected (i.e. if $J_{XX'} \ll J_{AA'}$ and $J_{XX'} \ll \Delta J$), the system can be solved analytically.

As in the chemically inequivalent case, the longitudinal two-spin-order term does not experience any coherent magnetic evolution in the high-field case and so the time-dependent amplitude, $b_1(\tau)$, can be written as: $b_1(\tau) = \exp(-R_{1,I_z S_z}\tau)$, where $R_{1,I_z S_z}$ is the effective longitudinal two-spin-order NMR relaxation rate.

As all of the terms in the density matrix (Eq. 7) do not commute, the evolution of $b_2(\tau)$, $b_3(\tau)$, and $b_4(\tau)$ must be considered simultaneously, rather than sequentially. Using Eq. 6 and the Liouville-von-Neumann equation (Eq. 3) we can write down a series of coupled differential equations to describe the coherent magnetic evolution of the AA'XX' system. Here we have included a single effective zero-quantum NMR relaxation rate, R_{ZQ}, to

describe the NMR relaxation behaviour of the three exchanging states. This effective relaxation rate will depend on the individual relaxation rates for the three states, as well as the rate of exchange between the zero-quantum coherences, ZQ_x and $2ZQ_y(T_z - R_z)$, and the longitudinal term, $2\frac{1}{2}(I_z - S_z)(T_z - R_z)$.

$$db_2(\tau)/d\tau = -2\pi\Delta J\, b_3(\tau) - R_{ZQ}b_2(\tau) \tag{8a}$$

$$db_3(\tau)/d\tau = 2\pi\Delta J b_2(\tau) - 2\pi J_{AA'} b_4(\tau) - R_{ZQ}b_3(\tau) \tag{8b}$$

$$db_4(\tau)/d\tau = 2\pi J_{AA'} b_3(\tau) - R_{ZQ}b_4(\tau) \tag{8c}$$

This system of coupled equations is directly related to the case of two strongly-coupled, chemically-inequivalent p-H$_2$-derived ^{1}H nuclei in low magnetic field (AB spin system) that has been solved previously by Natterer and Bargon for the initial conditions $b_2(0) = 1$ and $b_3(0) = b_4(0) = 0$.[11] Here the difference in chemical shift, $\delta\omega$, is replaced by the difference in J coupling between the hydrides and the heteronuclei: ΔJ. The solution to this system of equations is given in Eq. 9, where $\xi = \Delta J/J_{AA'}$ and $\omega = 2\pi\sqrt{J_{AA'}^2 + \Delta J^2}$. It should be noted that the amplitude of the $2ZQ_y(T_z - R_z)$ term, $b_3(\tau)$, has the opposite sign in our result compared to the amplitude of ZQ_y in the result of Natterer and Bargon.[11] The signs in the differential equations in Eq. 8 and the solutions in Eq. 9 are in agreement with the sign conventions used in the equations throughout this paper.

$$b_2(\tau) = \frac{1}{1+\xi^2}(1 + \xi^2 \cos\omega\tau)\exp(-R_{ZQ}\tau) \tag{9a}$$

$$b_3(\tau) = \frac{\xi}{\sqrt{1+\xi^2}}\sin\omega\tau \exp(-R_{ZQ}\tau) \tag{9b}$$

$$b_4(\tau) = \frac{\xi}{1+\xi^2}(1 - \cos\omega\tau)\exp(-R_{ZQ}\tau) \tag{9c}$$

The amplitudes b_2, b_3 and b_4 oscillate during the pump probe delay at angular frequency $\omega = 2\pi\sqrt{J_{AA'}^2 + \Delta J^2}$. The contributions of the three terms in Eq. 9 to the overall density matrix is controlled by the ratio $\xi = \Delta J/J_{AA'}$, which quantifies the relative strength of the hydride-hydride coupling. In a very strongly coupled system, in which ξ is small but non-zero, the final term in Eq. 7, with amplitude b_4, will dominate the density matrix.

15

C. NMR signal detection

To probe the evolution of the density matrix during the pump-probe delay, we can apply any appropriately adapted NMR pulse sequence at a fixed time, τ, following a single laser pulse (Figure 1a). The simplest detection pulse sequence consists of a single broadband (non-selective) ^{1}H rf pulse of tip angle, θ_1, applied at a time τ after the laser shot (Figure 1b). The pulse rotates the ZQ magnetic states that make up the density matrix during the pump-probe delay into a combination of NMR observable (single-quantum, SQ) and NMR silent (double-quantum, DQ, and ZQ) states. The evolution of the SQ terms can be recorded as a free induction decay (FID) and Fourier Transformed to generate a high-resolution ^{1}H NMR spectrum. The effect of a single ^{1}H pulse of tip angle, θ_1, on each of the states generated in the chemically inequivalent case (AX, AXY, AXYZ, Eq. 5) and the magnetically inequivalent case (AA'XX', Eq. 7) is summarized in Eq. S1 in the supporting information.

Using the results in Eq. S1, we can derive expressions for the single-quantum (SQ) density matrix (i.e. the NMR observable part) following the application of the rf pulse, $\rho_{SQ}(\tau^+)$, where τ^+ is used to denote the time immediately following the rf pulse. Here we assume that the rotations associated with the rf pulse are ideal and instantaneous. This approximation is only valid if the rf pulse duration is much shorter than the period of the oscillations of the zero-quantum coherences during the pump-probe delay. A single rf pulse, θ_2, can also be applied to the X channel, either instead of, or in addition to, the ^{1}H rf pulse (Figure 1c). This rf pulse will rotate the T_z and R_z terms by an angle θ_2 in the usual way.

More complex pulse sequences, such as the OPSY (Only *Para*hydrogen SpectroscopY) family of sequences, which use the principles of multiple-quantum filtration with gradient pulses to selectively observe ZQ, DQ or higher-order coherences,[79, 80] or selective excitation of only one of the hydride resonances,[33] can also be used to observe the different contributions to the p-H$_2$-enhanced NMR signals.

1. Chemical inequivalence (AX, AXY, AXYZ)

The SQ density matrix for an AXY spin system following the application of simultaneous, non-selective rf pulses of tip angle θ_1 to the ^{1}H nuclei (I and S) and θ_2 to T is presented in Eq. 10.

$$\rho_{SQ}^{AXY}(\tau^+) = -A_1(\tau)\tfrac{1}{2}(2I_xS_z + 2I_zS_x) + A_2(\tau)\tfrac{1}{2}(2I_yS_z - 2I_zS_y)$$

$$-A_3(\tau)\tfrac{1}{2}(2I_xS_z + 2I_zS_x)T_z + A_4(\tau)\tfrac{1}{2}(2I_yS_z - 2I_zS_y)T_z - A_5(\tau)\tfrac{1}{2}(4I_zS_zT_x) \quad (10\text{a})$$

$A_1(\tau) =$

$$\left[\exp(-R_{1,I_zS_z}\tau) - \exp(-R_{2,ZQ}\tau)\tfrac{1}{2}(\cos([\delta\omega + \pi\Delta J]\tau) + \cos([\delta\omega - \pi\Delta J]\tau))\right]\tfrac{1}{2}\sin 2\theta_1$$

$$(10\text{b})$$

$$A_2(\tau) = \tfrac{1}{2}(\sin([\delta\omega + \pi\Delta J]\tau) + \sin([\delta\omega - \pi\Delta J]\tau))\exp(-R_{2,ZQ}\tau)\sin\theta_1 \quad\quad (10\text{c})$$

$$A_3(\tau) = \tfrac{1}{2}(\cos([\delta\omega + \pi\Delta J]\tau) - \cos([\delta\omega - \pi\Delta J]\tau))\exp(-R_{2,ZQ}\tau)\tfrac{1}{2}\sin 2\theta_1 \cos\theta_2 \quad (10\text{d})$$

$$A_4(\tau) = \tfrac{1}{2}(\sin([\delta\omega + \pi\Delta J]\tau) - \sin([\delta\omega - \pi\Delta J]\tau))\exp(-R_{2,ZQ}\tau)\sin\theta_1 \cos\theta_2 \quad\quad (10\text{e})$$

$$A_5(\tau) = \tfrac{1}{2}(\cos([\delta\omega + \pi\Delta J]\tau) - \cos([\delta\omega - \pi\Delta J]\tau))\exp(-R_{2,ZQ}\tau)\sin^2\theta_1 \sin\theta_2 \quad\quad (10\text{f})$$

In the absence of a difference in coupling to a third nucleus (ΔJ = 0, AX spin system) or under the influence of Y decoupling during signal acquisition, $A_3 = A_4 = A_5 = 0$ and the density matrix is significantly simplified. The amplitudes of the observable terms, A_1 and A_2, are proportional to the amplitudes of the longitudinal two-spin order, ZQ_x, and ZQ_y terms in the density matrix immediately prior to the *rf* pulse. A_1 is equal to the difference in amplitude of the longitudinal two-spin-order and ZQ_x terms, while A_2 reflects the amplitude of the ZQ_y coherence. Note: in a singlet-triplet basis, $\{|S_0\rangle, |T_0\rangle, |T_{+1}\rangle, |T_{-1}\rangle\}$, the amplitude difference between the two-spin-order and ZQ_x terms is the amplitude of $|T_0\rangle\langle T_0|$.

If we define the observation operator as the sum:

$$I_{obs} = (I_x + S_x) + i(I_y + S_y), \quad\quad\quad\quad (11)$$

we can predict the form of the NMR spectrum that will arise from each term in Eq. 10 as shown in Figure 2.

(a) $2I_xS_z + 2I_zS_x$ (b) $2I_yS_z - 2I_zS_y$ (c) $I_x + S_x$
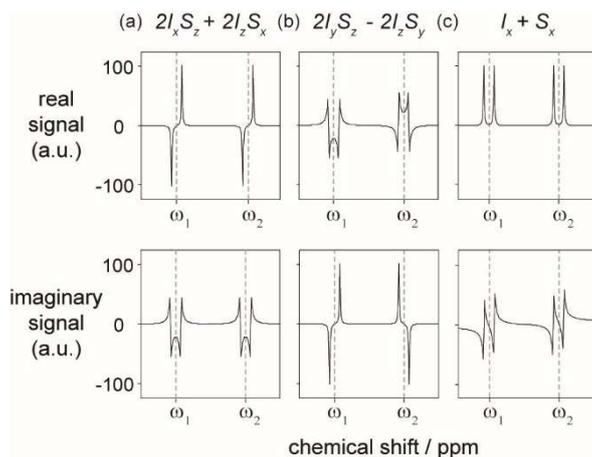
Figure 2. Simulated peaks for the real and imaginary components of an ^{1}H NMR spectrum obtained from the evolution of the density matrix, ρ, under the influence of an AX Hamiltonian (Eq. 4, $\Delta J = 0$), where (a) $\rho(0) = 2I_xS_z + 2I_zS_x$, (b) $\rho(0) = 2I_yS_z - 2I_zS_y$, and (c) $\rho(0) = I_x + S_x$, corresponding to standard thermally polarised NMR signals. The doublet splitting in the spectra is the homonuclear coupling, J_{AX}.

The first term in Eq. 10a gives rise to anti-phase peaks for each hydride in the real part of the spectrum with a corresponding pair of anti-phase dispersion peaks in the imaginary part (Figure 2a). The second term gives rise to anti-phase hydride peaks in the imaginary part of the spectrum and a pair of dispersion peaks in the real part (Figure 2b). Any contribution from thermal magnetization (of the form $I_x + S_x$) will give rise to a pair of in-phase doublets in the real part and a corresponding set of dispersion peaks in the imaginary part (Figure 2c). In other words, each contribution to the density matrix will produce two doublets centred on the chemical shift of the A and X spins, respectively, but the relative phases of these peaks will be different in each case. In addition, the amplitudes of the hyperpolarised contributions (A_1 and A_2) depend on the *rf* pulse angle θ_1 in different ways. A_1 is proportional to $\frac{1}{2}\sin 2\theta_1$, while A_2 is proportional to $\sin \theta_1$. Therefore there are several methods that can be used to differentiate between the various contributions to the NMR signal.

If we apply an *rf* pulse with tip angle: $\frac{n\pi}{2}$, where n is any odd integer (i.e. odd multiples of 90°), the ZQ_x and longitudinal two-spin-order terms will produce a combination of NMR-silent ZQ and DQ terms, while the ZQ_y term will be rotated into NMR-observable SQ terms. A FID recorded following this pulse will therefore contain information about the amplitude of the ZQ_y coherence exclusively, and have the form of Figure 2b. In contrast, a

18

DQ or ZQ quantum filtered OPSY sequence[80] can be used to selectively probe the difference in amplitude between the ZQ_x and longitudinal two-spin-order term and will produce an NMR spectrum of the form shown in Figure 2a.

If we apply an *rf* pulse that is *not* odd integer multiples of 90° ($\theta_1 = 45°$, for example) the SQ density matrix will contain a mixture of both terms in Eq. 10. However, we can exploit the differences in the relative phases of the hydride signals to isolate the contribution of each term to the density matrix through selective integration. To illustrate this behaviour, we first define the integral, $A(\omega)$, of a peak centred at $\omega' = \omega$, over an integration range given by Δ.

$$A(\omega) = \int_{\omega - \frac{\Delta}{2}}^{\omega + \frac{\Delta}{2}} s(\omega')d\omega', \tag{12}$$

The individual contributions of the two terms in Eq. 10 to the observed NMR spectrum, A_1 and A_2, can be calculated according to Eq. 13, where Re[] and Im[] indicate the real and the imaginary parts, respectively, and A_0 is a normalisation factor.

$$A_1 = A_0 \text{Re}[A(\omega_A + \pi J_{AX}) - A(\omega_A - \pi J_{AX}) + A(\omega_X + \pi J_{AX}) - A(\omega_X - \pi J_{AX})] \tag{13a}$$

$$A_2 = A_0 \text{Im}[A(\omega_A + \pi J_{AX}) - A(\omega_A - \pi J_{AX}) - A(\omega_X + \pi J_{AX}) + A(\omega_X - \pi J_{AX})] \tag{13b}$$

This integration method has the advantage of minimizing errors in the spectral baseline and cancels any hydride signals originating from thermal magnetization if the anti-phase peaks are well resolved, i.e. for $\Delta < 2\pi J_{AX}$.

If a series of 1D ^{1}H pump-probe NMR spectra are acquired with different delays, τ, they can be Fourier Transformed to produce a 2D spectrum, where the indirect dimension corresponds to evolution during the pump-probe delay (Figure 3a). In this 2D NMR spectrum, we would expect the first term in Eq. 10a to give rise to peaks at $f_1 = \pm\delta\omega/2\pi$ and $f_1 = 0$ Hz because it is modulated by $[1 - \cos(\delta\omega\tau)]$, while the second term in Eq. 10a will only give rise to peaks at $f_1 = \pm\delta\omega/2\pi$ because it is modulated by $\sin(\delta\omega\tau)$. As described previously, the relative contributions of these two terms to the 2D spectrum can be controlled by the choice of flip angle, θ_1. In practice, a flip angle of $\theta_1 = 90°$ is preferred because it generates observable NMR signals from the second term in Eq. 10a, exclusively, and so significantly simplifies the interpretation of the 2D spectrum.
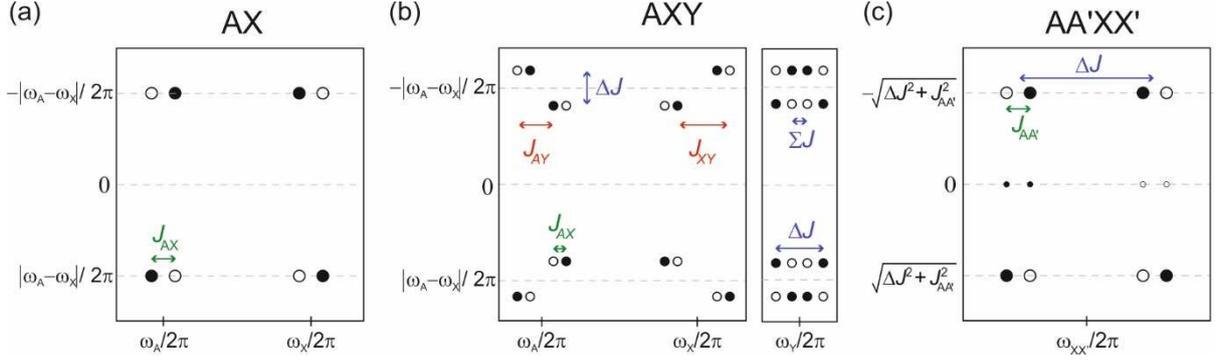
Figure 3. Predicted peak patterns in 2D pump-probe NMR spectra for (a) AX, (b) AXY, and (c) AA'XX' spin systems. (a) Excitation (θ_1 = 90°) and detection on the AX (^{1}H) channel. (b) Left: excitation (θ_1 = 90°) and detection on the AX (^{1}H) channel, right: simultaneous AX and Y excitation ($\theta_1 = \theta_2$ = 90°) followed by Y-detection. The 'X'-shaped peak pattern in the ^{1}H-detected spectrum corresponds to the case where J_{AY} and J_{XY} have opposite signs. (c) Excitation (θ_2 = 90°) and detection on the XX' channel. $\Sigma J = J_{trans} + J_{cis} = J_{A'X} + J_{AX} = J_{AX'} + J_{A'X'}$ and $\Delta J = J_{trans} - J_{cis} = J_{A'X} - J_{AX} = J_{AX'} - J_{A'X'}$. Negative and positive peak intensities are represented by open and filled circles, respectively.

In the absence of Y decoupling, the evolution of the amplitudes of the various terms in Eq. 10 will be modulated by any difference in coupling to the third spin, Y, and will depend on the state of this spin. The amplitude of the peaks that correspond to the spin-up state of Y, ($\langle T_z \rangle = +\frac{1}{2}$) will evolve with a frequency of: $\delta\omega/2\pi + \Delta J/2$, while the amplitude of the peaks associated with the spin-down state ($\langle T_z \rangle = -\frac{1}{2}$) will evolve with an oscillation frequency of: $\delta\omega/2\pi - \Delta J/2$. In a 2D pump-probe NMR spectrum this will correspond to a pair of doublets in the indirect dimension at $\pm\delta\omega/2\pi$ with a splitting equal to ΔJ, as illustrated in Figure 3b. If there are other heteronuclear or homonuclear spins that couple to the hydrides, additional splittings will be observed in the indirect dimension of the 2D ^{1}H pump-probe NMR spectrum, which will give rise to the same peak multiplet patterns as seen in standard NMR spectroscopy. However, the peak separation will be equal to the *difference* in J coupling between each hydride and the additional nucleus.

The coupling of the hydrides to an additional spin provides an opportunity to observe p-H$_2$-derived hyperpolarisation on this spin. In other words, we can probe the transfer of spin order from the p-H$_2$-derived hydrides to other nuclei. Only the final term in Eq. 10 will give rise to observable signal for Y. This signal will be at a maximum for tip angles: $\theta_1 = \theta_2$ = 90°. In the indirect dimension of the resultant 2D pump-probe NMR spectrum

20

we will observe peaks at $f_1 = \pm(\delta\omega/2\pi \pm \Delta J/2)$ due to the cosine modulation during the pump-probe delay. In the direct dimension, we will observe a pair of peaks separated by the sum of the scalar couplings ($\Sigma J = J_{AY} + J_{XY}$) and a pair of peaks of the opposite sense separated by the difference between the couplings ($\Delta J = J_{AY} - J_{XY}$). This is illustrated by the coupling pattern on the right in Figure 3b and is most readily apparent when Y is a heteronucleus.

2. Magnetic inequivalence (AA'XX')

The SQ density matrix for an AA'XX' spin system following the application of a non-selective ¹H *rf* pulse of tip angle θ_1 is presented in Eq. 14.

$$\rho_{SQ}^{AA'XX'}(\tau^+) = -B_1(\tau)\tfrac{1}{2}(2I_xS_z + 2I_zS_x) + B_2(\tau)\tfrac{1}{2}(2I_yS_z - 2I_zS_y)2(T_z - R_z)$$

$$-B_3(\tau)(I_x - S_x)(T_z - R_z) \tag{14a}$$

$$B_1(\tau) = \left[\exp(-R_{1,I_zS_z}\tau) - \tfrac{1}{1+\xi^2}(1 + \xi^2\cos\omega\tau)\exp(-R_{ZQ}\tau)\right]\tfrac{1}{2}\sin 2\theta_1 \tag{14b}$$

$$B_2(\tau) = \tfrac{\xi}{\sqrt{1+\xi^2}}\sin\omega\tau\,\exp(-R_{ZQ}\tau)\sin\theta_1 \tag{14c}$$

$$B_3(\tau) = \tfrac{\xi}{1+\xi^2}(1 - \cos\omega\tau)\exp(-R_{ZQ}\tau)\sin\theta_1 \tag{14d}$$

The first two terms are analogous to the AX case, where the difference in chemical shift is now replaced by the coupling term $\omega = 2\pi\sqrt{\Delta J^2 + J_{AA'}^2}$. The final product, which involves two spin order terms across all four nuclei, will only be significant in the case of a strongly coupled spin system. In the indirect dimension of a 2D pump-probe spectrum of the A spins (I and S), this term will give rise to peaks at $f_1 = \pm\omega/2\pi = \pm\sqrt{\Delta J^2 + J_{AA'}^2}$ and at $f_1 = 0$. The amplitude of these peaks, relative to the dominant peaks arising from the first two terms, is determined by the ratio: $\xi = \Delta J/J_{AA'}$.

If we instead apply an *rf* pulse, θ_2, to the X spins (T and R) then the SQ density matrix of the spin system immediately following the pulse will be as follows.

$$\rho_{SQ,X}^{AA'XX'}(\tau^+) = -\left[\tfrac{\xi}{\sqrt{1+\xi^2}}\sin\omega\tau\,\exp(-R_{ZQ}\tau)\sin\theta_2\right]2ZQ_y(T_x - R_x)$$

$$-\left[\tfrac{\xi}{1+\xi^2}(1 - \cos\omega\tau)\exp(-R_{ZQ}\tau)\sin\theta_2\right]2(I_z - S_z)(T_x - R_x) \tag{15}$$

Due to the strong coupling between the hydrides, the two terms in Eq. 15 will interconvert with a frequency equal to the coupling between A spins, $J_{AA'}$ and observable signals will be seen in the X nucleus 2D pump-probe spectrum. The first term will result in a spectrum in the direct dimension that contains an anti-phase doublet of anti-phase doublets, with splittings of ΔJ and $J_{AA'}$, respectively. These peaks will appear at frequencies of $f_1 = \pm\omega/2\pi$ in the indirect dimension. The second term will give rise to an anti-phase doublet of doublets with the same splittings: ΔJ (anti-phase) and $J_{AA'}$ (in-phase). These peaks will appear at $f_1 = \pm\omega/2\pi$ and $f_1 = 0$ in the indirect (τ evolution) dimension. The relative amplitudes of these two contributions to the 2D NMR spectrum will depend on ξ. The expected peak patterns for a 2D pump-probe spectrum of this type are illustrated in Figure 3c.

III. Experimental Methods

All NMR spectra were recorded on a Bruker Avance widebore 600 MHz spectrometer fitted with a BBO probe. Laser photolysis was carried out with a pulsed Nd:YAG laser (Continuum Surelite II) fitted with a frequency tripling crystal (output 355 nm). Operating conditions were typically: flash lamp voltage of 1.49 kV and Q-switch delay of 150 μs delivering 29.8 mJ per pulse. The unfocused laser beam is directed at the base of the spectrometer and reflected up into the probe via a mirror. Adjustment screws control the vertical and horizontal position of the mirror which is on a kinematic mount. The system is fully shielded from the operator and the screws of the kinematic mount can be adjusted remotely. The laser radiation is incident on a fixed mirror that is level with the sample and passes through a hole in the probe onto the NMR tube. Standard NMR tubes fitted with Young's taps were used. The samples contained 1–2 mg of compound and approximately 0.4 mL of solvent to give a concentration of between 3-6 mM. The synthesis details and NMR characterization for the complexes are provided in the supporting information.

Hydrogen enriched in the *para* spin state to > 99% was prepared by cooling H_2 to 27 K over activated charcoal using a system previously described in the literature.[33]

Standard NMR pulse sequences were modified for use with *p*-H_2 by including a synchronized laser initiation sequence prior to NMR excitation and detection (Figure 1a). A purpose-written program was used to control the laser firing from the NMR console with the laser set on external triggering. The fire signals are sent to the laser via a BNC

cable. The NMR pulse is initiated at a set delay time (τ) following the fire signal. The delay between sending the fire signal from the spectrometer and the actual firing of the laser pulse is controlled by a digital delay pulse generator (Stanford Research Systems Inc.) and was verified by a photodiode and an oscilloscope to be 150 μs. This signal delay was incorporated into the pulse sequence such that synchronized measurements with a time delay, τ, were achieved by setting the spectrometer delay to: τ + 150 μs. The precision of this delay between the laser and *rf* pulses is controlled by the 200 ns clock of the spectrometer. The 90° *rf* pulse durations were 13.5 μs for the ^{1}H channel and 8.4 μs for ^{31}P. All laser-pump, NMR probe spectra were acquired in a single scan, i.e. without the use of signal averaging.

IV. Results and Discussion

The validity of our model for the evolution of p-H$_2$-derived spin order following oxidative addition of p-H$_2$ at a metal centre can be tested experimentally using our pump-probe approach with systems where the rate of oxidative addition of p-H$_2$ to the transition metal complex is much faster than the magnetic evolution of the system. We have chosen to work with ruthenium dihydride complexes, where the rates of H$_2$ addition (Scheme 1) at 3 bar H$_2$ are expected to be on the order of $k = 10^6$ s^{-1} on the basis of flash photolysis measurements,[31, 81-83] several orders of magnitude faster than the corresponding hydride chemical shift/J coupling differences (tens to thousands of Hz). The three ruthenium dihydride complexes investigated here (Scheme 3) exemplify the different types of spin systems described above (AX, AXY, AXYZ and AA'XX') and so can be used to fully validate the model. NMR characterisation data and synthetic procedures for all complexes are provided in the supporting information.
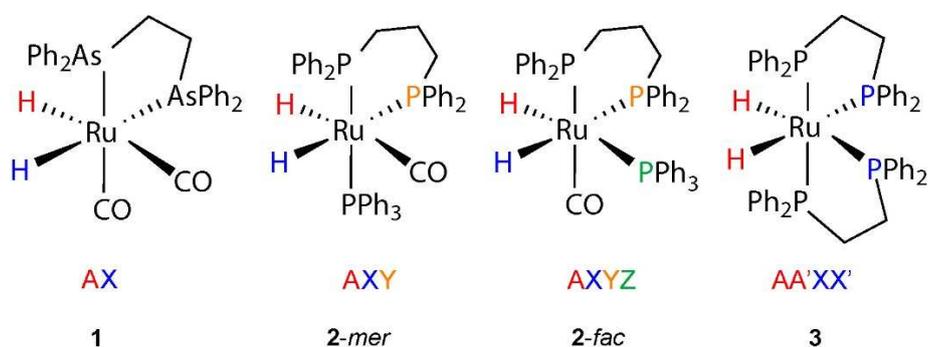
Scheme 3. The ruthenium dihydride complexes used in this study.

A. AX spin system

In the transition metal complex Ru(H)$_2$(CO)$_2$(dpae) (dpae = Ph$_2$AsCH$_2$CH$_2$AsPh$_2$) (**1** in Scheme 3), the hydrides are chemically inequivalent, with a difference in chemical shift ranging from 0.2 to 0.4 ppm in three common NMR solvents (Figure 4a-c). The 1D pump-probe ^{1}H NMR spectra (θ_1 = 90°) of **1** in Figure 4(a-c) indicate that the hydrides do not experience any appreciable *J* couplings to other nuclei in the complex, making this a good model for an isolated AX spin system (J_{AX} = 4.5 Hz). Furthermore, the range of chemical shift values in the three different solvents provides the opportunity to evaluate the theoretical model in a very controlled way.

A series of 1D pump-probe ^{1}H NMR spectra were acquired, where a single laser pulse was followed after a period τ by a single *rf* pulse with θ_1 = 45°. The 45° *rf* pulse allowed us to probe the evolution of all contributions to the density matrix during the pump-probe delay in a single set of experiments. The hydride peaks in the resultant series of 1D ^{1}H NMR spectra were integrated according to Eq. 13 to determine the time-dependence of the amplitude of the real (A_1, Figure 4g-i) and imaginary (A_2, Figure 4d-f) components of the signal during the pump-probe delay. The real part (A_1) corresponds to the difference in amplitude between the longitudinal two-spin order and ZQ_x terms and the imaginary part (A_2) corresponds to the amplitude of the ZQ_y term. A fit to the theoretical expressions in Eq. 10 (red lines in Figure 4; fit parameters in Table 1) reveals, as expected, that the oscillation frequency is equal to the differences in chemical shift given in Figure 4a-c. The high quality of the fits confirms the validity of our model and also highlights the fact that the pump-probe measurements are reproducible and quantitative. The solvent-dependent chemical shift differences allow for three independent validation measurements with the same complex. We note that on the timescale of these experiments, there was little observable relaxation (see Section D for relaxation time measurements).

Table 1. Parameters for fits of Eqs. 10 and 13 to the data in Figure 4 (red lines).

	1 in C$_6$D$_6$	**1** in C$_6$D$_{12}$	**1** in THF-d$_8$
Imaginary part (A_2)			
$\delta\omega/2\pi$ / Hz	241.4 ± 0.1	173.7 ± 0.1	117.6 ± 0.1
Real part (A_1)			
$\delta\omega/2\pi$ / Hz	241.5 ± 0.1	173.7 ± 0.1	117.9 ± 0.1

A series of 1D pump-probe NMR spectra can be Fourier transformed to yield a 2D spectrum as in Figure 4j ($\theta_1 = 90°$) and 4k ($\theta_1 = 45°$). For $\theta_1 = 90°$ (Figure 4j), we only detect NMR signals arising from the ZQ_y term and so we observe anti-phase peaks at $f_1 = \pm\delta\omega/2\pi = \pm241$ Hz (see Figure 3a). However for $\theta_1 = 45°$ (Figure 4k) we detect NMR signals arising from both terms in Eq. 10 and so peaks are also observed at $f_1 = 0$ Hz, with destructive interference leading to partial-signal cancelation at $f_1 = \pm\delta\omega/2\pi = \pm241$ Hz. A comparison between Figures 4j and 4k demonstrates the advantage of using $\theta_1 = 90°$, which gives rise to a 2D spectrum that is more easily interpreted.
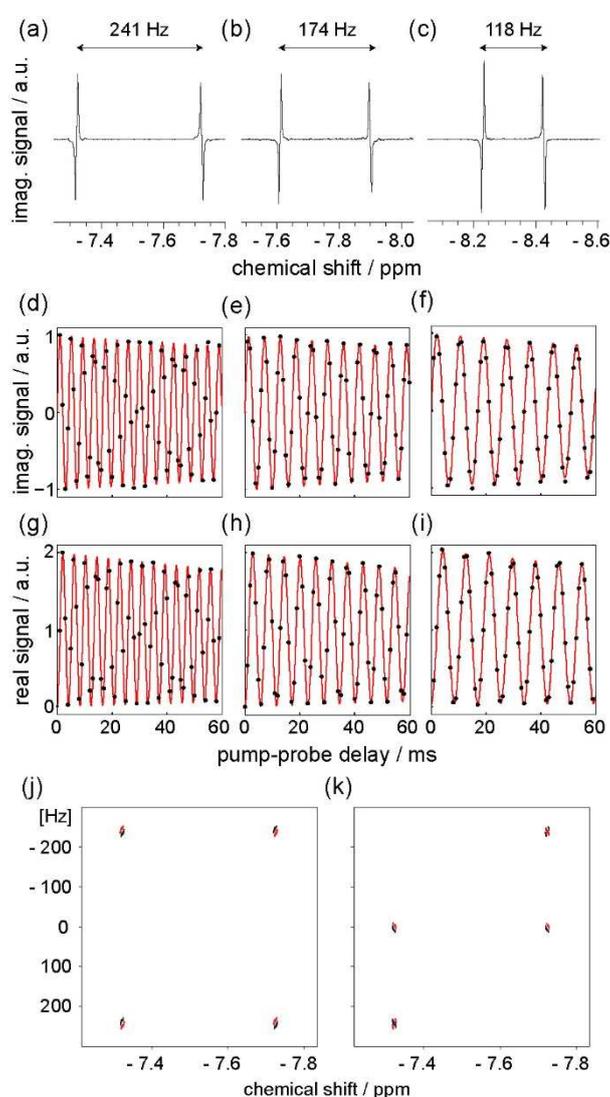
Figure 4. Hydride region of 1D pump-probe ^{1}H NMR spectra of **1** in (a) C_6D_6, (b) cyclohexane-d$_{12}$, and (c) THF-d$_8$, with $\tau = 1$ ms and $\theta_1 = 90°$. Integral of the hydride signals of **1** in the three solvents calculated from pump-probe ^{1}H NMR spectra ($\theta_1 = 45°$, $0 \leq \tau \leq$

60 ms) according to Eq. 13b (d-f) and Eq. 13a (g-i). Red lines are fits to the theoretical expressions for the amplitudes A$_1$ and A_2 in Eq. 10; parameters are listed in Table 1. (j,k) 2D ^{1}H pump-probe NMR spectra of **1** in C$_6$D$_6$ acquired with (j) θ_1 = 90° and (k) θ_1 = 45°. Positive intensity is plotted in black and negative intensity in red.

B.   AXY and AXYZ spin systems

As a model of an AXY spin system, we studied the complex Ru(H)$_2$(CO)(PPh$_3$)(dppp) (dppp = Ph$_2$PCH$_2$CH$_2$CH$_2$PPh$_2$) (**2** in Scheme 3) in C$_6$D$_6$, which has a major *mer* isomer and a minor *fac* isomer that is only observed in the photochemical pump, NMR probe experiment. Coupling constants and chemical shifts for the two isomers of **2** are available in Table S2 of the supporting information. The *mer* isomer has a single ^{31}P nucleus coordinated to the metal in the same plane as the two hydrides, and two mutually *trans* ^{31}P nuclei. The couplings between the mutually *trans* ^{31}P and each of the hydrides are the same within a few Hz; therefore these couplings play only a very minor role in the evolution during the pump-probe delay on the timescale of our experiment. Thus, this isomer is a good model of an AXY spin system (Scheme 1b). The *fac* isomer has three ^{31}P nuclei coordinated to the metal, two *trans* to a hydride proton and a third *trans* to a CO ligand. This third ^{31}P couples similarly (to within a few Hz) to both hydride protons and so does not play a significant role in the evolution during the pump-probe delay. Therefore, we can consider this isomer to be an AXYZ spin system. The NMR signals corresponding to the *fac* isomer are absent in a thermally polarised ^{1}H NMR spectrum (top in Figure 5a), but hyperpolarised signals for both isomers are visible (*mer* δ -6.51 and -7.00, red; *fac* δ -6.95 and -7.95, blue) in the 1D ^{1}H pump-probe NMR spectrum (bottom in Figure 5a, τ = 0.5 ms, θ_1 = 90°).
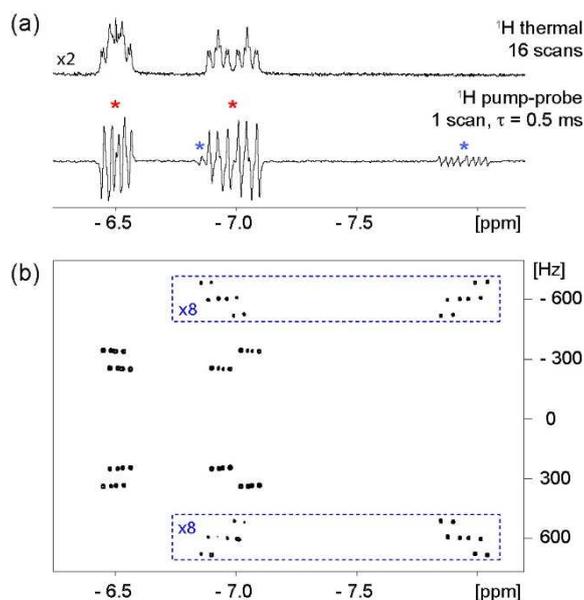
Figure 5. ^{1}H NMR spectra of **2** in C_6D_6 (3 atm p-H$_2$.) (a) Hydride region of 1D ^{1}H NMR spectra acquired with thermal polarisation (top, 16 scans) and p-H$_2$-enhancement (bottom, acquired using Fig. 1b, $\theta_1 = 90°$, $\tau = 0.5$ ms, 1 scan). Both the *mer* (red stars) and *fac* (blue stars) isomers are observed in the hyperpolarised spectrum. (b) 2D ^{1}H pump-probe NMR spectrum ($0 \leq \tau \leq 50$ ms, $\theta_1 = 90°$, magnitude mode). The intensity inside the blue boxes has been increased by a factor of 8 so that the signals from both isomers are visible with the same set of contour levels.

The 2D ^{1}H pump-probe NMR spectrum in Figure 5b displays p-H$_2$ enhanced peaks for both isomers of **2**. The difference in chemical shift of the two hydrides is far greater for the *fac* than for the *mer* isomer ($\delta\omega_{mer} = 2\pi * 293$ Hz and $\delta\omega_{fac} = 2\pi * 600$ Hz) and so there is a separation of the overlapping peaks at δ 7.0 in the indirect (τ evolution) dimension of the 2D spectrum. As predicted by Eq. 13, the *mer* isomer (AXY spin system) gives rise to a doublet in the indirect (τ evolution) dimension with peaks at $f_1 = \pm250\pm5$ Hz and $\pm339\pm5$ Hz, in good agreement with the predicted frequencies of $\pm \delta\omega/2\pi \pm \Delta J/2$ (see Table 2 for tabulated values.) The coordination of a second ^{31}P nucleus to the metal in the same plane as the hydrides effectively renders the *fac* isomer an AXYZ spin system (see above). In direct analogy with the well-known multiplicity rules of NMR spectroscopy, the scalar coupling between the hydrides and the two ^{31}P nuclei gives rise to doublet of doublets, which resembles a triplet due to the similarity of the hydride-^{31}P coupling differences. In the 2D spectrum, the peaks occur at $f_1 = \pm516$ Hz, ±600 Hz, and ±684 Hz, in good agreement with predicted values (see Table 2).

Table 2 Comparison of the oscillation frequencies during the pump-probe delay as measured from the 2D pump-probe spectra in Figures 5-8 with those predicted from chemical shifts and coupling constants (Table S2 and S3 in the supporting information.)

	2-*mer* in C_6D_6		2-*fac* in C_6D_6			3 in C_6D_6
Obs. / Hz	250 ± 5	339 ± 5	516 ± 5	600 ± 5	684 ± 5	84 ± 5
Pred. / Hz	249.8	338.2	517.4	600.1	682.8	83.9

As predicted, ^{31}P hyperpolarisation can be observed if *rf* pulses are applied to the ^1H and ^{31}P channels simultaneously (Figure 6). The 2D ^{31}P pump-probe NMR spectrum in Figure 6 was acquired under the influence of selective decoupling of the aromatic and CH_2 protons in order to simplify the spectra and limit signal cancellation due to the overlap of positive and negative peaks. We note that under the conditions employed here (2 kHz waltz-64 ^1H decoupling applied at 4 ppm) the hydride-phosphorus couplings appear to have been reduced by 8% relative to the values obtained from a fully coupled ^1H spectrum (see supporting information for numerical simulations).
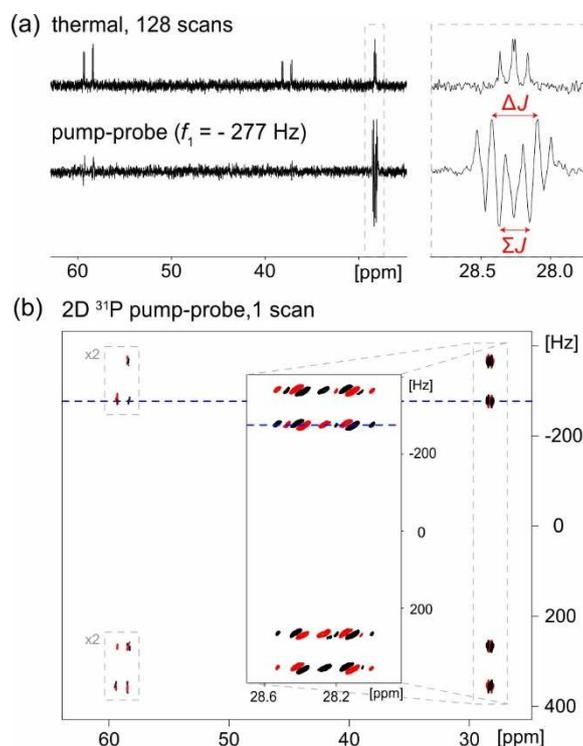
Figure 6. ^{31}P NMR spectra of **2**-*mer* in toluene-d_8 (3 atm *p*-H_2, 295 K). (a) (top) 1D $^{31}P\{^1H\}$ NMR spectrum acquired with thermal polarisation and 128 scans, (bottom) 1D profile from the 2D ^{31}P pump-probe NMR spectrum in (b), taken along the dashed red line at f_1

= -277 Hz. (b) 2D ^{31}P pump-probe NMR spectrum acquired using the pulse sequence in Fig. 1c with simultaneous excitation of the ^{1}H and ^{31}P spins ($\theta_1 = \theta_2 = 90^{\circ}$) and selective decoupling of the non-hydride ^{1}H resonances during ^{31}P acquisition (2 kHz waltz-64 at 4 ppm). Hyperpolarisation is observed for both the in-plane ^{31}P nucleus (δ 28.3) and one of the mutually-*trans* ^{31}P nuclei (δ 58.8, dppp), where the latter ^{31}P signals have been increased by a factor of 2 within the dashed boxes.

In the pump-probe ^{31}P spectra in Figure 6 we observe hyperpolarisation on the in-plane ^{31}P nucleus (δ 28.3) at $f_1 = \pm272\pm5$ Hz and $\pm360\pm5$ Hz, which is in good agreement with the predicted frequencies $f_1 = \delta\omega/2\pi \pm \Delta J/2 = \pm273.8$ Hz and ±362.2 Hz ($\delta\omega/2\pi = 318$ Hz (0.53 ppm), $\Delta J = 88.4$ Hz for **2**-*mer* in toluene-d_8). In the direct dimension, the doublet of doublets due to the homonuclear phosphorus coupling is further split by the hydride-phosphorus couplings. We observe two positive sets of peaks, separated by the difference between the hydride-phosphorus couplings ($\Delta J = 88.4$ Hz,) and an additional two sets of negative peaks, separated by the sum of the hydride-phosphorus couplings ($\Sigma J = 55.6$ Hz). Partial signal cancellation has occurred due to the overlap of positive and negative peaks. The ^{31}P linewidth is strongly dependent on the efficiency of the selective decoupling of the non-hydride ^{1}H nuclei in the complex (particularly the *ortho* protons of the phenyl groups and the CH_2 protons on the bridge of the chelating phosphine.) Therefore, we expect that improved decoupling would result in the observation of larger ^{31}P enhancements. Homonuclear decoupling of the mutually-trans ^{31}P nuclei would also reduce signal cancellation due to overlapping peaks and so could be used to increase the intensity of the observed ^{31}P signal.

Interestingly, we also observe a small amount of hyperpolarisation on the ^{31}P at δ 58.8 (dppp), which has a difference in coupling to the hydrides of 4.5 Hz. The ^{31}P at δ 38.6 (PPh$_3$) has a difference in coupling of only 1.2 Hz and so no hyperpolarisation is observed for this nucleus on the timescale of the experiment ($0 \leq \tau \leq 58.8$ ms).

Hyperpolarisation of the ^{31}P signal was also observed in pump-probe NMR spectra of **2** in C$_6$D$_6$ following the application of a *rf* pulse of $\theta_2 = 90°$ to the ^{31}P channel when continuous broadband *rf* irradiation was applied to the ^{1}H spins during the acquisition of the ^{31}P signal (Figure 7). As in Figure 5, a doublet is observed in the indirect dimension at $f_1 = \delta\omega/2\pi \pm \Delta J/2$ ($f_1 = \pm246\pm5$ Hz and $\pm336\pm5$ Hz). The observation of ^{31}P hyperpolarisation in this case can be understood as follows. Immediately following the

application of the single pulse to the heteronucleus (applied along y with a tip angle, θ_2) the single-quantum density matrix will be:

$$\rho_{SQ}^{AXY}(\tau^+) = -\frac{1}{2}(\cos[(\delta\omega + \pi\Delta J)\tau] - \cos[(\delta\omega - \pi\Delta J)\tau])\sin\theta_2\, 2ZQ_xT_x$$

$$+\frac{1}{2}(\sin[(\delta\omega + \pi\Delta J)\tau] - \sin[(\delta\omega - \pi\Delta J)\tau])\sin\theta_2\, 2ZQ_yT_x. \tag{16}$$

Under the influence of continuous wave (cw) irradiation applied to the hydride resonances, with an amplitude of ω_1, $2ZQ_xT_x$ will evolve according to Eq. 17.

$$2ZQ_xT_x \xrightarrow{\omega_1(I_x+S_x)t_2} 2I_yS_yT_x\cos\omega_1t_2 + 2I_zS_zT_x\sin\omega_1t_2 + 2I_xS_xT_x \tag{17}$$

The second term in Eq. 17 will evolve into an anti-phase doublet of anti-phase doublets under the influence of the effective difference in heteronuclear J coupling between the two hydrides and the Y spin under the influence of the spin-lock field. It is this residual coupling that gives rise to the small anti-phase splitting ($\sim$ 2 Hz) observed in Figure 7. This residual coupling is essential for the observation of hyperpolarisation in this case. The residual coupling is much smaller than the linewidth of the ^{31}P{^{1}H} peaks in a thermal spectrum (see Figure 7a). This confirms that a significant amount of signal cancellation has occurred, limiting the amount of observable ^{31}P hyperpolarisation.
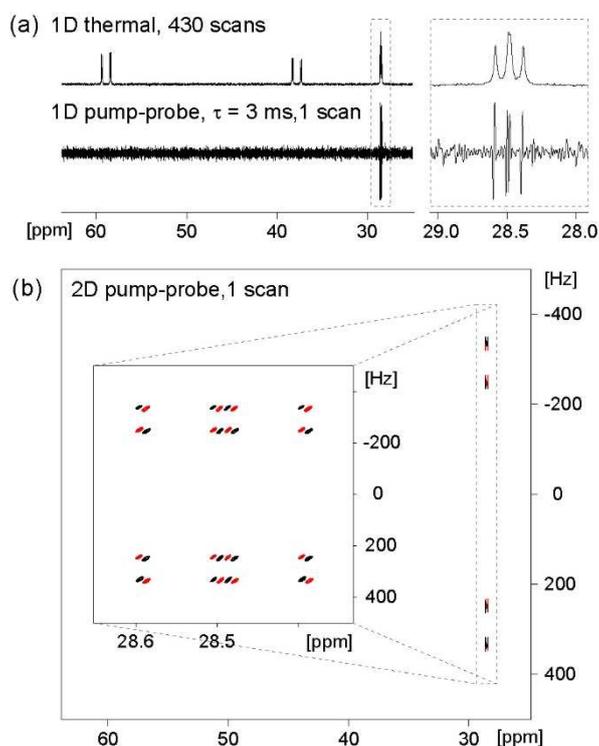
Figure 7. ^{31}P{^{1}H} NMR spectra of **2**-*mer* in C$_6$D$_6$ (3 atm p-H$_2$) (a) Thermally polarised 1D

$^{31}P\{^1H\}$ NMR spectrum (top, 430 scans) and p-H$_2$-enhanced $^{31}P\{^1H\}$ NMR spectrum (bottom, θ_1 = 0, θ_2 = 90°, τ = 3 ms, 1 scan). A zoomed view of the in-plane ^{31}P peaks is shown to the right. (b) 2D $^{31}P\{^1H\}$ acquired with the pulse sequence in Figure 1c (2 kHz GARP decoupling, θ_1 = 0, θ_2 = 90°, 0 ≤ τ ≤ x). The in-plane ^{31}P (δ 28.5) is the only nucleus to receive appreciable p-H$_2$-hyperpolarisation on the timescale of the experiment.

C. AA'XX' spin system

As a model of an AA'XX' spin system, we studied cis-Ru(H)$_2$(dppe)$_2$ (dppe = Ph$_2$PCH$_2$CH$_2$PPh$_2$) (**3** in Scheme 3) in C$_6$D$_6$. Coupling constants and chemical shifts for **3** are available in Table S3 of the supporting information. In this complex, the hydrides are chemically equivalent but magnetically inequivalent by virtue of the difference in the $J(^1H,^{31}P)_{cis}$ and $J(^1H,^{31}P)_{trans}$ couplings to a pair of chemically equivalent ^{31}P nuclei coordinated to the metal in the same plane. The hydrides also couple to a pair of chemically equivalent ^{31}P nuclei coordinated to the metal in a mutually $trans$ position; however the couplings between each hydride and the mutually $trans$ ^{31}P are not significantly different and so these ^{31}P nuclei do not play a key role in the pump-probe experiment. In addition, the homonuclear J coupling between the in-plane ^{31}P nuclei is much smaller than the difference in the heteronuclear couplings and the ^1H homonuclear coupling ($J_{XX'} \ll \Delta J$; $J_{XX'} \ll J_{AA'}$). Therefore the analytical solutions for this spin system developed in section II.B.2 can be applied here.

For this AA'XX' spin system we predict that there will be two contributions to a 2D pump-probe NMR spectrum following a 90° rf pulse applied to either the ^1H spins (AA') or the ^{31}P spins (XX'). The major component, which corresponds to the first term in Eq. 15, will consist of peaks at $f_1 = \pm\omega/2\pi = \pm\sqrt{\Delta J^2 + J_{AA'}^2} = 83.9$ Hz in the indirect dimension due to the modulation by $\sin\omega\tau$ during the pump-probe delay. The minor component, which corresponds to the second term in Eq. 15, will give rise to peaks at $f_1 = \pm\omega/2\pi = \pm\sqrt{\Delta J^2 + J_{AA'}^2} = 83.9$ Hz and $f_1 = 0$ Hz in the indirect dimension due to the $(1 - \cos\omega\tau)$ modulation during the pump-probe delay. In previous work, we published a 2D pump-probe ^1H NMR spectrum for **3** that displayed major peaks at $f_1 = \pm84$ Hz in the indirect (pump-probe) dimension,[34] as predicted by the theoretical treatment in section II.B.2. In addition, we showed that ^{31}P hyperpolarisation was observed when a 90° pulse was applied exclusively to the ^{31}P channel prior to signal acquisition. In contrast to the ^1H spectrum, the 2D ^{31}P pump-probe NMR spectrum displayed major peaks at $f_1 = \pm84$ and

at $f_1 = 0$ Hz. Furthermore, the lines were too broad to interpret the spectral features in the direct dimension. The theoretical development presented above suggests that, as in the ^{1}H spectrum, the ^{31}P pump-probe spectrum for an AA'XX' spin system should display a major component at $f_1 = \pm\omega/2\pi = \pm\sqrt{\Delta J^2 + J_{AA'}^2}$ due to the sinusoidal modulation of the second term in Eq. 15 during the pump probe delay. A much smaller contribution to the ^{31}P spectrum is expected at $f_1 = \pm\omega/2\pi = \pm\sqrt{\Delta J^2 + J_{AA'}^2}$ and at $f_1 = 0$ Hz due to the third term in Eq. 15, which is modulated by $(1 - \cos\delta\omega\tau)$. The relative contribution of this term is determined by the parameter, $\zeta = \Delta J / J_{AA'}$ (~6% in this case). Figure 8a presents a 2D pump-probe ^{31}P NMR spectrum acquired with selective decoupling of the non-hydride ^{1}H resonances during signal acquisition. This selective decoupling significantly narrows the ^{31}P resonances and therefore limits signal cancellation due to the overlap of anti-phase peaks. The resultant 2D pump-probe spectrum contains major peaks at $f_1 = \pm 84$ Hz as expected. The contributions from the first and second terms in Eq. 15, can be analysed by taking lines from the 2D spectrum at $f_1 = \pm 84$ Hz and $f_1 = 0$ Hz. The difference of the first two spectra ($f_1 = \pm 84$ Hz) reveals the contribution of the first term in Eq. 15 (top in Figure 8c), which is modulated by a sinusoidal oscillation during the pump-probe delay. The sum of these spectra ($f_1 = \pm 84$ Hz, Figure 8c (middle)) as well as the third spectrum ($f_1 = 0$ Hz, Figure 8c, bottom) reveal the contribution from the second term in Eq. 15, which is modulated by $(1 - \cos\omega\tau)$ during τ. While the first term is clearly dominant (top in Figure 8c), the relative intensities of the peaks arising from the second term is larger than the 6% predicted by the relative J couplings in the system. This is likely due to signal cancellation of the anti-phase peaks associated with the dominant term (Figure 8c, top).

(a) 2D pump-probe ^{31}P{^{1}H}$_{sel}$

(b) thermal ^{31}P{^{1}H}, 32 scans

(c) pump-probe ^{31}P{^{1}H}$_{sel}$

$S(-\omega) - S(+\omega)$

$S(-\omega) + S(+\omega)$

$S(0)$
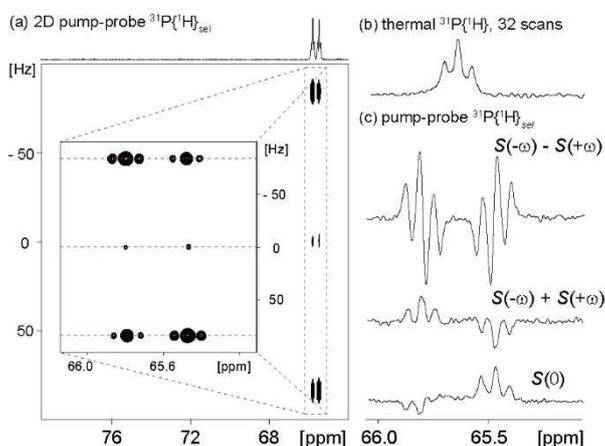
Figure 8. ^{31}P NMR spectra of **3** in C$_6$D$_6$ (3 *atm p*-H$_2$) (a) 2D pump-probe ^{31}P{^{1}H}$_{sel}$ NMR spectrum acquired with θ_1 = 0, θ_2 = 90°, 2 kHz waltz-64 decoupling at 4 ppm during acquisition and $0 \leq \tau \leq 50$ ms. (b) In-plane ^{31}P region of a thermal 1D ^{31}P{^{1}H} NMR spectrum of **3** acquired with 32 scans. (c) 1D slices of the 2D spectrum in (a) calculated as (top) the difference between the slice at f_1 = -84 Hz and f_1 = +84 Hz, (middle) the sum of the slices at f_1 = -84 Hz and f_1 = +84 Hz, and (bottom) 1D slice at f_1 = 0 Hz.

D. NMR Relaxation

The relaxation times for the ZQ coherences, $T_{2,ZQ}$, and the longitudinal two-spin-order term, T_{1,I_zS_z}, were determined for the three ruthenium di-hydrides **1**, **2**, and **3** in C$_6$D$_6$ (3 atm *p*-H$_2$, 295 K) using the pulse sequence presented in Figure 1d. In this pulse sequence, the fixed delay Δ immediately following the laser pulse maximises the evolution of the initial *p*-H$_2$-derived singlet state into observable triplet states. In the case of an AX spin system this delay is set to $\Delta = 1/(4\delta v)$ such that the density matrix at the end of this delay contains contributions from only the longitudinal two-spin order term and ZQ_y. In the case of the AA'XX' system, the delay is set to $\Delta = 1/(4\Delta J)$. The fixed delay is followed by an echo, where a broadband 180° pulse is used to refocus any evolution of the ZQ_y coherence due to a difference in chemical shift between the hydrides and/or a difference in *J*-coupling between the hydride and other heteronuclei in the complex. This echo is not strictly necessary in order to measure the relaxation rates; however, it is convenient because it allows for the use of arbitrary pump-probe delays without the need to fully sample the ZQ coherence evolution frequencies. For the measurements of **2**, broadband ^{31}P decoupling was applied during signal acquisition to simplify the hydride region of the ^{1}H NMR spectra and improve the signal-to-noise.

The relaxation rate of the various spin states can be determined in a single pseudo-2D experiment by repeating the pulse sequence in Figure 1d for a range of echo times, τ, with $\theta_y = 45°$. If the initial delay Δ is well calibrated, the density matrix at the end of the echo period will only contain contributions from ZQ_y and $\frac{1}{2}2I_zS_z$. Spectra acquired following a 45° pulse can therefore be divided into contributions from the zero quantum coherence and the longitudinal two-spin order term through the selective integration of the hydride peaks as outlined in section II.C.1 (see Eq. 13). A summary of the relaxation times for the three complexes together with thermal (single-quantum) T_1 values, measured using a standard inversion recovery sequence, are reported in Table 3.

Table 3 Summary of relaxation times of the three complexes used in this study (in C_6D_6, 295 K, 3 atm p-H_2).

Complex	T_{1,I_zS_z} / ms	$T_{2,ZQ}$ / ms	T_1 / ms
1	1630 ± 30	265 ± 8	1900 ± 100 (δ -7.34) 1500 ± 100 (δ -7.74)
2-*mer*	461 ± 110	158 ± 21	830 ± 130 (δ -7.0) 680 ± 90 (δ -6.5)
3	301 ± 27	96 ± 15	420 ± 20 (δ -8.33)

For the three complexes examined in this work, we observed minimal ^{1}H relaxation on the timescale of the magnetic oscillations during the pump-probe delay. This was because, as illustrated in Table 3, all three complexes have relaxation times on the order of 100 ms or longer, while the period of oscillation of the NMR signals ranged from 3 – 12 ms. However, such comparatively long relaxation times are not a requirement of the method. In order to observe hyperpolarisation using the pump-probe approach, it is only necessary that the zero-quantum relaxation times are equal to or longer than the period of the magnetic oscillations that give rise to observable NMR signals (i.e $T_{1,I_zS_z}, T_{2,ZQ} \geq 2\pi/(\delta\omega)$ for chemically inequivalent hydrides or $T_{1,I_zS_z}, T_{2,ZQ} \geq (\Delta J)^{-1}$ for magnetically inequivalent hydrides). Therefore, in contrast to the time averaged PHIP approach, in the synchronised pump-probe method it is possible to observe p-H_2 hyperpolarisation for systems with zero-quantum relaxation times down to a few milliseconds. This was illustrated in the case of the complex $Ru(H)_2(CO)(PPh_3)_3$ in Ref. [34], where hyperpolarisation was observed despite zero-quantum relaxation times on the order of 3 ms.

V.   Conclusions

In this work, we have explored the use of laser pump, NMR probe spectroscopy with *para*hydrogen hyperpolarisation to directly observe the evolution of p-H_2-derived spin order for a range of coupling networks. The laser initiation step generates an ensemble of hyperpolarised product molecules in a coherent magnetic state, allowing us to follow the evolution of this state on a fast timescale (tens to hundreds of μs) without the need for a time-consuming *rf* preparation step. We have presented a theoretical framework to describe the coherent magnetic evolution of the initial p-H_2-derived singlet state when the p-H_2 protons form part of an AX, AXY, AXYZ, or AA'XX' spin system in the product

molecule. This model was validated through the study of three ruthenium dihydride complexes.

The complex $Ru(H)_2(CO)_2(dpae)$ **1**, a model for an AX spin system, was studied in three different NMR solvents for which the difference in chemical shift between the hydrides varies from 0.2 to 0.4 ppm (120 Hz to 240 Hz at 14 T). The magnetic oscillations observed during the pump-probe delay fit the predicted behaviour for all terms in the density matrix with a high degree of accuracy, demonstrating both the validity of our model and the reproducibility of the pump-probe technique.

2D ^1H and ^{31}P pump-probe NMR spectra of the complex $Ru(H)_2(CO)(PPh_3)(dppp)$ **2** were presented where the second dimension corresponds to evolution during the probe delay. These spectra were found to be in excellent agreement with our theoretical predictions for an AXY spin system. Both the major *mer* and minor *fac* isomers of **2** were observed in the hyperpolarised ^1H NMR spectra. The coupling patterns observed for the two isomers demonstrated the difference between the behaviour of an AXY and an AXYZ spin system and further validated our theoretical model. In accordance with the predictions, ^{31}P hyperpolarisation was observed for the *mer* isomer following simultaneous 90° *rf* excitation pulses applied to both the ^{31}P and ^1H nuclei. ^{31}P hyperpolarisation was also observed following the application of a single 90° pulse to the ^{31}P channel when broadband *rf* irradiation was applied to the ^1H channel during ^{31}P signal acquisition.

The complex *cis*-$Ru(H)_2(dppe)_2$ **3** was studied as a model of an AA'XX' system, where the former *p*-H_2 ^1H's are chemically equivalent but magnetically inequivalent via the difference in *J* coupling to a pair of chemically-equivalent ^{31}P nuclei. A 2D ^{31}P pump-probe NMR spectrum of **3** was presented, where selective ^1H decoupling of the non-hydride resonances was used to narrow the ^{31}P lines such that anti-phase signal cancellation was reduced. The resultant high-resolution 2D ^{31}P spectrum displayed the same features as the 2D ^1H pump-probe spectrum (published previously) [34] in agreement with predictions from our theoretical analysis.

In all of these examples, we considered the evolution of the *p*-H_2-derived nuclear spin states in the product molecule in the high-field regime and in the absence of *rf* irradiation during the pump-probe delay. However, this method could be extended to probe the transfer of *p*-H_2-derived polarisation directly in a range of different scenarios. Of particular interest would be the transfer of polarisation via *rf* irradiation in the high

field[74, 78] and the spontaneous transfer of polarisation in the low-field regime, which has direct implications for optimising hyperpolarisation using the signal amplification by reversible exchange (SABRE) methodology.[10]

In this work we have focused exclusively on the use of p-H$_2$ as the source of the hyperpolarised long-lived nuclear spin state. However, p-H$_2$ is just one of a growing number of examples of molecules that contain nuclei in a LLS.[42, 55, 84] Therefore this method is not fundamentally limited to the study of reactions of H$_2$ but could also be used to monitor the reactivity of any molecule that contains nuclei prepared in a LLS, as long as the reaction can be initiated photochemically and the symmetry of the nuclei in the LLS is broken in a suitable way in the product molecule.

Acknowledgments

References

[1]   P. Nikolaou, B.M. Goodson, E.Y. Chekmenev, NMR Hyperpolarization Techniques for Biomedicine, Chem.-Eur. J., 21 (2015) 3156-3166.

[2]   T.R. Carver, C.P. Slichter, Polarization of Nuclear Spins in Metals, Physical Review, 92 (1953) 212-213.

[3]   A.W. Overhauser, Polarization of Nuclei in Metals, Physical Review, 92 (1953) 411-415.

[4]   J.H. Ardenkjaer-Larsen, B. Fridlund, A. Gram, G. Hansson, L. Hansson, M.H. Lerche, R. Servin, M. Thaning, K. Golman, Increase in Signal-to-Noise Ratio of > 10,000 Times in Liquid-State NMR, Proc. Natl. Acad. Sci. U. S. A., 100 (2003) 10158-10163.

[5]   L.R. Becerra, G.J. Gerfen, R.J. Temkin, D.J. Singel, R.G. Griffin, Dynamic Nuclear-Polarization with a Cyclotron-Resonance Maser at 5-T, Phys. Rev. Lett., 71 (1993) 3561-3564.

[6]   T.G. Walker, W. Happer, Spin-Exchange Optical Pumping of Noble-Gas Nuclei, Rev. Mod. Phys. , 69 (1997) 629-642.

[7]   C.R. Bowers, D.P. Weitekamp, Para-Hydrogen and Synthesis Allow Dramatically Enhanced Nuclear Alignment, J. Am. Chem. Soc., 109 (1987) 5541-5542.

[8]   C.R. Bowers, D.P. Weitekamp, Transformation of Symmetrization Order to

Nuclear-Spin Magnetization by Chemical-Reaction and Nuclear-Magnetic-Resonance, Phys. Rev. Lett., 57 (1986) 2645-2648.

[9]   T.C. Eisenschmid, R.U. Kirss, P.P. Deutsch, S.I. Hommeltoft, R. Eisenberg, J. Bargon, R.G. Lawler, A.L. Balch, Para Hydrogen Induced Polarization in Hydrogenation Reactions, J. Am. Chem. Soc., 109 (1987) 8089-8091.

[10]   R.W. Adams, J.A. Aguilar, K.D. Atkinson, M.J. Cowley, P.I.P. Elliott, S.B. Duckett, G.G.R. Green, I.G. Khazal, J. Lopez-Serrano, D.C. Williamson, Reversible Interactions with Para-Hydrogen Enhance NMR Sensitivity by Polarization Transfer, Science, 323 (2009) 1708-1711.

[11]   J. Natterer, J. Bargon, Parahydrogen Induced Polarization, Prog. Nucl. Magn. Reson. Spectrosc., 31 (1997) 293-315.

[12]   R.A. Green, R.W. Adams, S.B. Duckett, R.E. Mewis, D.C. Williamson, G.G.R. Green, The Theory and Practice of Hyperpolarization in Magnetic Resonance Using Parahydrogen, Prog. Nucl. Magn. Reson. Spectrosc., 67 (2012) 1-48.

[13]   S.B. Duckett, C.L. Newell, R. Eisenberg, More Than Inept - Parahydrogen and Inept+ Give Unprecedented Resonance Enhancement to C-13 by Direct H-1 Polarization Transfer, J. Am. Chem. Soc., 115 (1993) 1156-1157.

[14]   U. Bommerich, T. Trantzschel, S. Mulla-Osman, G. Buntkowsky, J. Bargon, J. Bernarding, Hyperpolarized F-19-Mri: Parahydrogen-Induced Polarization and Field Variation Enable F-19-Mri at Low Spin Density, Phys. Chem. Chem. Phys., 12 (2010) 10309-10312.

[15]   M. Haake, J. Natterer, J. Bargon, Efficient NMR Pulse Sequences to Transfer the Parahydrogen-Induced Polarization to Hetero Nuclei, J. Am. Chem. Soc., 118 (1996) 8688-8691.

[16]   L.T. Kuhn, U. Bommerich, J. Bargon, Transfer of Parahydrogen-Induced Hyperpolarization to F-19, J. Phys. Chem. A, 110 (2006) 3521-3526.

[17]   S. Aime, R. Gobetto, F. Reineri, D. Canet, Hyperpolarization Transfer from Parahydrogen to Deuterium Via Carbon-13, J. Chem. Phys., 119 (2003) 8890-8896.

[18]   K.D. Atkinson, M.J. Cowley, P.I.P. Elliott, S.B. Duckett, G.G.R. Green, J. Lopez-Serrano, A.C. Whitwood, Spontaneous Transfer of Parahydrogen Derived Spin Order to Pyridine at Low Magnetic Field, J. Am. Chem. Soc., 131 (2009) 13362-13368.

[19]   R.W. Adams, S.B. Duckett, R.A. Green, D.C. Williamson, G.G.R. Green, A Theoretical Basis for Spontaneous Polarization Transfer in Non-Hydrogenative Parahydrogen-Induced Polarization, J. Chem. Phys., 131 (2009) 194505.

[20]   S.B. Duckett, C.J. Sleigh, Applications of the Parahydrogen Phenomenon: A

Chemical Perspective, Prog. Nucl. Magn. Reson. Spectrosc., 34 (1999) 71-92.

[21]   S.B. Duckett, R.E. Mewis, Application of Parahydrogen Induced Polarization Techniques in NMR Spectroscopy and Imaging, Acc. Chem. Res., 45 (2012) 1247-1257.

[22]   R.H. Zhou, E.W. Zhao, W. Cheng, L.M. Neal, H.B. Zheng, R.E. Quinones, H.E. Hagelin-Weaver, C.R. Bowers, Parahydrogen-Induced Polarization by Pairwise Replacement Catalysis on Pt and Ir Nanoparticles, J. Am. Chem. Soc., 137 (2015) 1938-1946.

[23]   E.W. Zhao, H.B. Zheng, K. Ludden, Y. Xin, H.E. Hagelin-Weaver, C.R. Bowers, Strong Metal-Support Interactions Enhance the Pairwise Selectivity of Parahydrogen Addition over Ir/Tio2, Acs Catalysis, 6 (2016) 974-978.

[24]   K. Golman, O. Axelsson, H. Johannesson, S. Mansson, C. Olofsson, J.S. Petersson, Parahydrogen-Induced Polarization in Imaging: Subsecond C-13 Angiography, Magn. Reson. Med., 46 (2001) 1-5.

[25]   N.M. Zacharias, H.R. Chan, N. Sailasuta, B.D. Ross, P. Bhattacharya, Real-Time Molecular Imaging of Tricarboxylic Acid Cycle Metabolism in Vivo by Hyperpolarized 1-C-13 Diethyl Succinate, J. Am. Chem. Soc., 134 (2012) 934-943.

[26]   J.B. Hovener, N. Schwaderlapp, R. Borowiak, T. Lickert, S.B. Duckett, R.E. Mewis, R.W. Adams, M.J. Burns, L.A.R. Highton, G.G.R. Green, A. Olaru, J. Hennig, D. von Elverfeldtt, Toward Biocompatible Nuclear Hyperpolarization Using Signal Amplification by Reversible Exchange: Quantitative in Situ Spectroscopy and High-Field Imaging, Anal. Chem., 86 (2014) 1767-1774.

[27]   M. Goldman, H. Johannesson, Conversion of a Proton Pair Para Order into C-13 Polarization by Rf Irradiation, for Use in Mri, C. R. Phys., 6 (2005) 575-581.

[28]   C. Godard, P. Callaghan, J.L. Cunningham, S.B. Duckett, J.A.B. Lohman, R.N. Perutz, NMR Characterisation of Unstable Solvent and Dihydride Complexes Generated at Low Temperature by in-Situ UV Irradiation, Chem. Commun., 23 (2002) 2836-2837.

[29]   K.A.M. Ampt, S. Burling, S.M.A. Donald, S. Douglas, S.B. Duckett, S.A. Macgregor, R.N. Perutz, M.K. Whittlesey, Photochemical Isomerization of N-Heterocyclic Carbene Ruthenium Hydride Complexes: In Situ Photolysis, Parahydrogen, and Computational Studies, J. Am. Chem. Soc., 128 (2006) 7452-7453.

[30]   D. Schott, P. Callaghan, J. Dunne, S.B. Duckett, C. Godard, J.M. Goicoechea, J.N. Harvey, J.P. Lowe, R.J. Mawby, G. Muller, R.N. Perutz, R. Poli, M.K. Whittlesey, The Reaction of M(Co)(3)(Ph2pch2ch2pph2) (M = Fe, Ru) with Parahydrogen: Probing the Electronic Structure of Reaction Intermediates and the Internal Rearrangement Mechanism for the Dihydride Products, Dalton Trans., (2004)

3218-3224.

[31] M.V. Campian, R.N. Perutz, B. Procacci, R.J. Thatcher, O. Torres, A.C. Whitwood, Selective Photochemistry at Stereogenic Metal and Ligand Centers of Cis-Ru(Diphosphine)(2)(H)(2) : Preparative, NMR, Solid State, and Laser Flash Studies, J. Am. Chem. Soc., 134 (2012) 3480-3497.

[32] M.S. Anwar, D. Blazina, H.A. Carteret, S.B. Duckett, T.K. Halstead, J.A. Jones, C.M. Kozak, R.J.K. Taylor, Preparing High Purity Initial States for Nuclear Magnetic Resonance Quantum Computing, Phys. Rev. Lett., 93 (2004) 040501.

[33] D. Blazina, S.B. Duckett, T.K. Halstead, C.M. Kozak, R.J.K. Taylor, M.S. Anwar, J.A. Jones, H.A. Carteret, Generation and Interrogation of a Pure Nuclear Spin State by Parahydrogen-Enhanced NMR Spectroscopy: A Defined Initial State for Quantum Computation, Magn. Reson. Chem., 43 (2005) 200-208.

[34] O. Torres, B. Procacci, M.E. Halse, R.W. Adams, D. Blazina, S.B. Duckett, B. Eguillor, R.A. Green, R.N. Perutz, D.C. Williamson, Photochemical Pump and NMR Probe: Chemically Created NMR Coherence on a Microsecond Time Scale, J. Am. Chem. Soc., 136 (2014) 10124-10131.

[35] A.H. Zewail, Femtochemistry: Atomic-Scale Dynamics of the Chemical Bond Using Ultrafast Lasers - (Nobel Lecture), Angew. Chem., Int. Ed., 39 (2000) 2587-2631.

[36] R. Zhang, M. Newcomb, Laser Flash Photolysis Generation of High-Valent Transition Metal-Oxo Species: Insights from Kinetic Studies in Real Time, Acc. Chem. Res., 41 (2008) 468-477.

[37] J.M. Butler, M.W. George, J.R. Schoonover, D.M. Dattelbaum, T.J. Meyer, Application of Transient Infrared and near Infrared Spectroscopy to Transition Metal Complex Excited States and Intermediates, Coord. Chem. Rev., 251 (2007) 492-514.

[38] P. Kukura, D.W. McCamant, R.A. Mathies, Femtosecond Stimulated Raman Spectroscopy, in: Annu. Rev. Phys. Chem., 2007, pp. 461-488.

[39] E.T.J. Nibbering, H. Fidder, E. Pines, Ultrafast Chemistry: Using Time-Resolved Vibrational Spectroscopy for Interrogation of Structural Dynamics, in: Annu. Rev. Phys. Chem., 2005, pp. 337-367.

[40] W.R. Browne, J.J. McGarvey, The Raman Effect and Its Application to Electronic Spectroscopies in Metal-Centered Species: Techniques and Investigations in Ground and Excited States, Coord. Chem. Rev., 251 (2007) 454-473.

[41] B. Procacci, P.M. Aguiar, M.E. Halse, R.N. Perutz, S.B. Duckett, Photochemical Pump and NMR Probe to Monitor the Formation and Kinetics of Hyperpolarized Metal Dihydrides, Chem. Sci. , (2016) 7087-7093.

[42]   M.H. Levitt, Singlet Nuclear Magnetic Resonance, Annual Review of Physical Chemistry, Vol 63, 63 (2012) 89-105.

[43]   R. Sarkar, P. Ahuja, P.R. Vasos, G. Bodenhausen, Long-Lived Coherences for Homogeneous Line Narrowing in Spectroscopy, Phys. Rev. Lett., 104 (2010) 053001.

[44]   G. Stevanato, S.S. Roy, J. Hill-Cousins, I. Kuprov, L.J. Brown, R.C.D. Brown, G. Pileio, M.H. Levitt, Long-Lived Nuclear Spin States Far from Magnetic Equivalence, Phys. Chem. Chem. Phys., 17 (2015) 5913-5922.

[45]   G. Stevanato, J.T. Hill-Cousins, P. Hakansson, S.S. Roy, L.J. Brown, R.C.D. Brown, G. Pileio, M.H. Levitt, A Nuclear Singlet Lifetime of More Than One Hour in Room-Temperature Solution, Angew. Chem., Int. Ed., 54 (2015) 3740-3743.

[46]   G. Pileio, M.H. Levitt, Theory of Long-Lived Nuclear Spin States in Solution Nuclear Magnetic Resonance. II. Singlet Spin Locking, J. Chem. Phys., 130 (2009) 214501.

[47]   M. Carravetta, M.H. Levitt, Theory of Long-Lived Nuclear Spin States in Solution Nuclear Magnetic Resonance. I. Singlet States in Low Magnetic Field, J. Chem. Phys., 122 (2005) 214505.

[48]   W.S. Warren, E. Jenista, R.T. Branca, X. Chen, Increasing Hyperpolarized Spin Lifetimes through True Singlet Eigenstates, Science, 323 (2009) 1711-1714.

[49]   Y. Feng, T. Theis, T.-L. Wu, K. Claytor, W.S. Warren, Long-Lived Polarization Protected by Symmetry, J. Chem. Phys., 141 (2014) 134307.

[50]   Y. Feng, R.M. Davis, W.S. Warren, Accessing Long-Lived Nuclear Singlet States between Chemically Equivalent Spins without Breaking Symmetry, Nat. Phys., 8 (2012) 831-837.

[51]   R. Sarkar, P. Ahuja, P.R. Vasos, A. Bornet, O. Wagnieres, G. Bodenhausen, Long-Lived Coherences for Line-Narrowing in High-Field NMR, Prog. Nucl. Magn. Reson. Spectrosc., 59 (2011) 83-90.

[52]   S.J. DeVience, R.L. Walsworth, M.S. Rosen, Preparation of Nuclear Spin Singlet States Using Spin-Lock Induced Crossing, Phys. Rev. Lett., 111 (2013) 173002.

[53]   M. Carravetta, O.G. Johannessen, M.H. Levitt, Beyond the T-1 Limit: Singlet Nuclear Spin States in Low Magnetic Fields, Phys. Rev. Lett., 92 (2004) 153003.

[54]   M. Carravetta, M.H. Levitt, Long-Lived Nuclear Spin States in High-Field Solution NMR, J. Am. Chem. Soc., 126 (2004) 6228-6229.

[55]   A. Bornet, X. Ji, D. Mammoli, B. Vuichoud, J. Milani, G. Bodenhausen, S. Jannin, Long-Lived States of Magnetically Equivalent Spins Populated by Dissolution-DNP and Revealed by Enzymatic Reactions, Chemistry-a European Journal, 20 (2014)

17113-17118.

[56]   P.R. Vasos, A. Comment, R. Sarkar, P. Ahuja, S. Jannin, J.P. Ansermet, J.A. Konter, P. Hautle, B. van den Brandt, G. Bodenhausen, Long-Lived States to Sustain Hyperpolarized Magnetization, Proc. Natl. Acad. Sci. U. S. A., 106 (2009) 18469-18473.

[57]   A.M. Olaru, S.S. Roy, L.S. Lloyd, S. Coombes, G.G.R. Green, S.B. Duckett, Creating a Hyperpolarised Pseudo Singlet State through Polarisation Transfer from Parahydrogen under SABRE, Chem. Commun., 52 (2016) 7842-7845.

[58]   S.S. Roy, P.J. Rayner, P. Norcott, G.G.R. Green, S.B. Duckett, Long-Lived States to Sustain SABRE Hyperpolarised Magnetisation, Phys. Chem. Chem. Phys., 18 (2016) 24905-24911.

[59]   T. Theis, G.X. Ortiz, A.W.J. Logan, K.E. Claytor, Y. Feng, W.P. Huhn, V. Blum, S.J. Malcolmson, E.Y. Chekmenev, Q. Wang, W.S. Warren, Direct and Cost-Efficient Hyperpolarization of Long-Lived Nuclear Spin States on Universal N-15(2)-Diazirine Molecular Tags, Sci. Adv., 2 (2016) 7.

[60]   B. Eguillor, P.J. Caldwell, M.C.R. Cockett, S.B. Duckett, R.O. John, J.M. Lynam, C.J. Sleigh, I. Wilson, Detection of Unusual Reaction Intermediates During the Conversion of W(N-2)(2)(Dppe)(2) to W(H)(4)(Dppe)(2) and of H2o into H-2, J. Am. Chem. Soc., 134 (2012) 18257-18265.

[61]   C.R. Bowers, Sensitivity Enhancement Utilizing Parahydrogen, in: Emagres, John Wiley & Sons, Ltd, 2007.

[62]   M.G. Pravica, D.P. Weitekamp, Net NMR Alignment by Adiabatic Transport of Para-Hydrogen Addition-Products to High Magnetic-Field, Chem. Phys. Lett., 145 (1988) 255-258.

[63]   S. Schäublin, A. Wokaun, R.R. Ernst, Pulse Techniques Applied to Chemically-Induced Dynamic Nuclear-Polarization, J. Magn. Reson., 27 (1977) 273-302.

[64]   S. Schaublin, A. Wokaun, R.R. Ernst, Creation of Off-Diagonal Elements in Chemically-Induced Dynamic Nuclear-Polarization Experiments, Chem. Phys., 14 (1976) 285-293.

[65]   S. Schäublin, A. Hohener, R.R. Ernst, Fourier Spectroscopy of Nonequilibrium States, Application to CIDNP, Overhauser Experiments and Relaxation-Time Measurements, J. Magn. Reson., 13 (1974) 196-216.

[66]   A.N. Pravdivtsev, A.V. Yurkovskaya, K.L. Ivanov, H.M. Vieth, Importance of Polarization Transfer in Reaction Products for Interpreting and Analyzing CIDNP at Low Magnetic Fields, J. Magn. Reson., 254 (2015) 35-47.

[67]   S.M. Harper, L.C. Neil, I.J. Day, P.J. Hore, K.H. Gardner, Conformational Changes in a Photosensory Lov Domain Monitored by Time-Resolved NMR Spectroscopy, J. Am. Chem. Soc., 126 (2004) 3390-3391.

[68]   A.S. Kiryutin, O.B. Morozova, L.T. Kuhn, A.V. Yurkovskaya, P.J. Hore, H-1 and C-13 Hyperfine Coupling Constants of the Tryptophanyl Cation Radical in Aqueous Solution from Microsecond Time-Resolved CIDNP, J. Phys. Chem. B, 111 (2007) 11221-11227.

[69]   K.H. Mok, T. Nagashima, I.J. Day, J.A. Jones, C.J.V. Jones, C.M. Dobson, P.J. Hore, Rapid Sample-Mixing Technique for Transient NMR and Photo-CIDNP Spectroscopy: Applications to Real-Time Protein Folding, J. Am. Chem. Soc., 125 (2003) 12484-12492.

[70]   S. Perrier, E. Mugeniwabagara, A. Kirsch-De Mesmaeker, P.J. Hore, M. Luhmer, Exploring Photoreactions between Polyazaaromatic Ru(II) Complexes and Biomolecules by Chemically Induced Dynamic Nuclear Polarization Measurements, J. Am. Chem. Soc., 131 (2009) 12458-12465.

[71]   H. Johannesson, O. Axelsson, M. Karlsson, Transfer of Para-Hydrogen Spin Order into Polarization by Diabatic Field Cycling, C. R. Phys., 5 (2004) 315-324.

[72]   K.L. Ivanov, A.V. Yurkovskaya, H.M. Vieth, Coherent Transfer of Hyperpolarization in Coupled Spin Systems at Variable Magnetic Field, J. Chem. Phys., 128 (2008).

[73]   J.A. Pople, W.G. Schneider, H.J. Bernstein, The Analysis of Nuclear Magnetic Resonance Spectra .2. 2 Pairs of 2 Equivalent Nuclei, Canadian Journal of Chemistry-Revue Canadienne De Chimie, 35 (1957) 1060-1072.

[74]   T. Theis, M. Truong, A.M. Coffey, E.Y. Chekmenev, W.S. Warren, Light-SABRE Enables Efficient in-Magnet Catalytic Hyperpolarization, J. Magn. Reson., 248 (2014) 23-26.

[75]   T. Theis, M.L. Truong, A.M. Coffey, R.V. Shchepin, K.W. Waddell, F. Shi, B.M. Goodson, W.S. Warren, E.Y. Chekmenev, Microtesla SABRE Enables 10% Nitrogen-15 Nuclear Spin Polarization, J. Am. Chem. Soc., 137 (2015) 1404-1407.

[76]   K.L. Ivanov, A.N. Pravdivtsev, A.V. Yurkovskaya, H.M. Vieth, R. Kaptein, The Role of Level Anti-Crossings in Nuclear Spin Hyperpolarization, Prog. Nucl. Magn. Reson. Spectrosc., 81 (2014) 1-36.

[77]   L. Buljubasich, M.B. Franzoni, H.W. Spiess, K. Munnemann, Level Anti-Crossings in Parahydrogen Induced Polarization Experiments with Cs-Symmetric Molecules, J. Magn. Reson., 219 (2012) 33-40.

[78]   A.N. Pravdivtsev, A.V. Yurkovskaya, N.N. Lukzen, H.-M. Vieth, K.L. Ivanov, Exploiting Level Anti-Crossings (Lacs) in the Rotating Frame for Transferring Spin

Hyperpolarization, Phys. Chem. Chem. Phys., 16 (2014) 18707-18719.

[79] J.A. Aguilar, P.I.P. Elliott, J. Lopez-Serrano, R.W. Adams, S.B. Duckett, Only Para-Hydrogen Spectroscopy (OPSY), a Technique for the Selective Observation of Para-Hydrogen Enhanced NMR Signals, Chem. Commun., (2007) 1183-1185.

[80] J.A. Aguilar, R.W. Adams, S.B. Duckett, G.G.R. Green, R. Kandiah, Selective Detection of Hyperpolarized NMR Signals Derived from Para-Hydrogen Using the Only Para-Hydrogen Spectroscopy (OPSY) Approach, J. Magn. Reson., 208 (2011) 49-57.

[81] L. Cronin, M.C. Nicasio, R.N. Perutz, R.G. Peters, D.M. Roddick, M.K. Whittlesey, Laser Flash-Photolysis and Matrix-Isolation Studies of $Ru(R_2pch_2ch_2pr_2)_2(H)_2$ (R = C_2h_5, C_6h_5, C_2f_5) - Control of Oxidative Addition Rates by Phosphine Substituents, J. Am. Chem. Soc., 117 (1995) 10047-10054.

[82] M. Colombo, M.W. George, J.N. Moore, D.I. Pattison, R.N. Perutz, I.G. Virrels, T.Q. Ye, Ultrafast Reductive Elimination of Hydrogen from a Metal Carbonyl Dihydride Complex; a Study by Time-Resolved IR and Visible Spectroscopy, J. Chem. Soc., Dalton Trans., (1997) 2857-2859.

[83] R. Osman, R.N. Perutz, A.D. Rooney, A.J. Langley, Picosecond Photolysis of a Metal Dihydride - Rapid Reductive Elimination of Dihydrogen from Ru(Dmpe)(2)H-2 (Dmpe=(Ch3)(2)Pch2ch2p(Ch3)(2)), J. Phys. Chem., 98 (1994) 3562-3563.

[84] M.B. Franzoni, L. Buljubasich, H.W. Spiess, K. Muennemann, Long-Lived H-1 Singlet Spin States Originating from Para-Hydrogen in Cs-Symmetric Molecules Stored for Minutes in High Magnetic Fields, J. Am. Chem. Soc., 134 (2012) 10393-10396.